

8-30-2011

Microstructural, geochronologic and thermochronologic evidence for both Paleo- and Mesoproterozoic displacement across the Gneiss Canyon shear zone : lower Granite Gorge, Grand Canyon, Arizona

Jacob McDermott

Follow this and additional works at: https://digitalrepository.unm.edu/eps_etds

Recommended Citation

McDermott, Jacob. "Microstructural, geochronologic and thermochronologic evidence for both Paleo- and Mesoproterozoic displacement across the Gneiss Canyon shear zone : lower Granite Gorge, Grand Canyon, Arizona." (2011).
https://digitalrepository.unm.edu/eps_etds/52

This Thesis is brought to you for free and open access by the Electronic Theses and Dissertations at UNM Digital Repository. It has been accepted for inclusion in Earth and Planetary Sciences ETDs by an authorized administrator of UNM Digital Repository. For more information, please contact disc@unm.edu.

Jacob J. McDermott

Candidate

Earth and Planetary Sciences

Department

This thesis is approved, and it is acceptable in quality and form for publication:

Approved by the Thesis Committee:

Karl S. Karsten

Chairperson

James C. King

Michael P. Williams

by

THESIS

Submitted in Partial Fulfillment of the
Requirements for the Degree of

The University of New Mexico
Albuquerque, New Mexico

DEDICATION

To my parents for their unwavering support and gentle guidance.

ACKNOWLEDGEMENTS

I've been blessed with an excellent group of colleagues, without whose help this manuscript would likely not exist. Thank you to my committee for all that they have provided, especially my adviser Karl Karlstrom for his patience and resourcefulness. To Matt Heizler and Mike Williams for generously providing Ar-Ar, and monazite data respectively, and for their assistance with interpretation, thank you. To everyone who provided logistical support during field outings in the Lower Gorge, and helped navigate through the intricacies of departmental and UNM rules and protocol (Cindy), thanks for everything. Lastly, to everyone whose thoughtful insights and technical support improved this manuscript, especially Ryan Crow and the rest of the tectonics research group, thank you very much.

**MICROSTRUCTURAL, GEOCHRONOLOGIC AND
THERMOCHRONOLOGIC EVIDENCE FOR BOTH PALEO AND
MESOPROTEROZOIC DISPLACEMENT ACROSS THE GNEISS
CANYON SHEAR ZONE: LOWER GRANITE GORGE, GRAND
CANYON, ARIZONA**

by

Jacob J. McDermott

B.S., Geology, University of Pittsburgh at Johnstown 2006

M.S., Earth and Planetary Sciences, 2011

ABSTRACT

The Gneiss Canyon shear zone (GCSZ) in north-western Arizona sits between high grade migmatites on the west and lower amphibolite grade schists on the east. This 13 km-wide zone, contains domains of intense D_2 strain up to 100m wide that separate blocks of preserved northwest-striking D_1 fabric. Previous investigations of D_2 domains show west-side-up and dextral displacement forming at amphibolite grade. D_2 field and microstructures suggest deformation temperatures of >500 °C. Zoned monazite displays 1696 Ma cores and 1649 Ma outermost rims, suggesting protracted deformation associated with the Yavapai orogeny.

Newly described retrograde D_3 mylonites consists of discrete (cm to m-scale) zones, which occur within, and represent reactivation of the wider GCSZ. D_3 microstructures indicate lower temperature dynamic recrystallization of quartz, as well as brittle deformation suggesting temperatures of $<300-450$ °C. These D_3 domains within GCSZ also indicate west-side-up and/or dextral displacement, and could record retrograde shearing near the end of the Yavapai orogeny, or a younger shearing event (favored here).

$^{40}\text{Ar}/^{39}\text{Ar}$ data from Lower Granite gorge show disparate T-t paths for blocks on either side of the GCSZ. Both eastern and western blocks show initial ~1.7-~1.5 Ga cooling rate of ~2 °C/Ma, but with a 30-40 Ma time lag in cooling for the western block through muscovite closure (~350 °C). The disparity in biotite ages is greater. The eastern “cold” block cooled through biotite closure (~300 °C) at 1527 Ma; the western “hot” block apparently remained warmer, and cooled through ~300 °C by ~1400 Ma.

K-feldspar multiple diffusion domain modeling shows an inversion of relative cooling rates from ~300 °C to ~150 °C. Results from Spencer Canyon and Gold Butte indicate cooling from 300-200 °C between ~1.4 and ~1.2 Ga, then slow cooling from 200-150 °C between 1.2-0.8 Ga. Travertine Grotto K-feldspar modeling suggests cooling from ~300 °C at ~1300 Ma to ~200 °C by ~1100 Ma. This slower late cooling suggests burial of the Travertine Grotto block as a result of ~1.4 Ga west-side-up thrusting across the GCSZ. The combined data, suggests that D₃ shear zones record reactivation of the GCSZ during regional ~1.4 Ga magmatism and associated deformation.

TABLE OF CONTENTS

LIST OF FIGURES	viii
LIST OF TABLES	x
INTRODUCTION AND REGIONAL BACKGROUND.....	1
GEOLOGIC SETTING	7
STRUCTURAL GEOLOGY	16
<i>Methods</i>	<i>16</i>
<i>High temperature history of Lower Granite Gorge</i>	<i>19</i>
<i>Low temperature shear zones and their microstructures</i>	<i>23</i>
U-TH-PB MONAZITE DATING.....	27
<i>Methods and results</i>	<i>27</i>
<i>Microstructures of Monazite-dated sample.....</i>	<i>28</i>
⁴⁰AR/³⁹AR THERMOCHRONOLOGY	31
<i>Methods</i>	<i>31</i>
<i>Results.....</i>	<i>33</i>
DISCUSSION OF DIFFERENTIAL COOLING HISTORIES IN NORTH WESTERN ARIZONA.....	39
<i>Possible thermal effects of 1.4 Ga tectonism</i>	<i>44</i>
<i>Links between microstructures, geochronology, and Ar cooling paths.....</i>	<i>47</i>
CONCLUSIONS	49
REFERENCES CITED	51
APPENDIX--⁴⁰AR/³⁹AR DATA TABLES	59

LIST OF FIGURES

Figure 1. Proterozoic outcrop and proposed Paleoproterozoic crustal boundaries in north-western Arizona.....	2
Figure 2. Geologic map of northwestern Arizona and southeastern Nevada	6
Figure 3. Geologic sketch map of Proterozoic rocks of the Lower Granite Gorge	9
Figure 4. Schematic cross-section of Lower Granite Gorge.....	11
Figure 5. Field photographs of D_1 , D_2 fabrics in western Grand Canyon.....	14
Figure 6. High temperature microstructures observed in the Lower Granite Gorge	20
Figure 7. Field Photos of Low temperature (D_3) mylonites from RM 242.....	24
Figure 8. Photomicrographs of low temperature shear zones found within the Gneiss Canyon shear zone	26
Figure 9. Photomicrographs from sample W93LG236-B6.2	29
Figure 10. U-Th-Pb Monazite analysis results from sample W93LG236-B6.2.....	30
Figure 11. Hornblende $^{40}\text{Ar}/^{39}\text{Ar}$ spectra for the Lower Granite Gorge and Devil's Cove	34
Figure 12. Muscovite $^{40}\text{Ar}/^{39}\text{Ar}$ spectra for the Lower Granite Gorge.....	36
Figure 13. Biotite $^{40}\text{Ar}/^{39}\text{Ar}$ spectra for the Lower Granite Gorge and Devil's Cove.....	37
Figure 14. K-Feldspar $^{40}\text{Ar}/^{39}\text{Ar}$ spectra and MDD plots for the Lower Granite Gorge.....	38
Figure 15. Time Temperature plot for crustal blocks within study area.....	40

Figure 16. *Aeromagnetic map of northwestern Arizona with proposed province boundary lines and zones*

..... 46

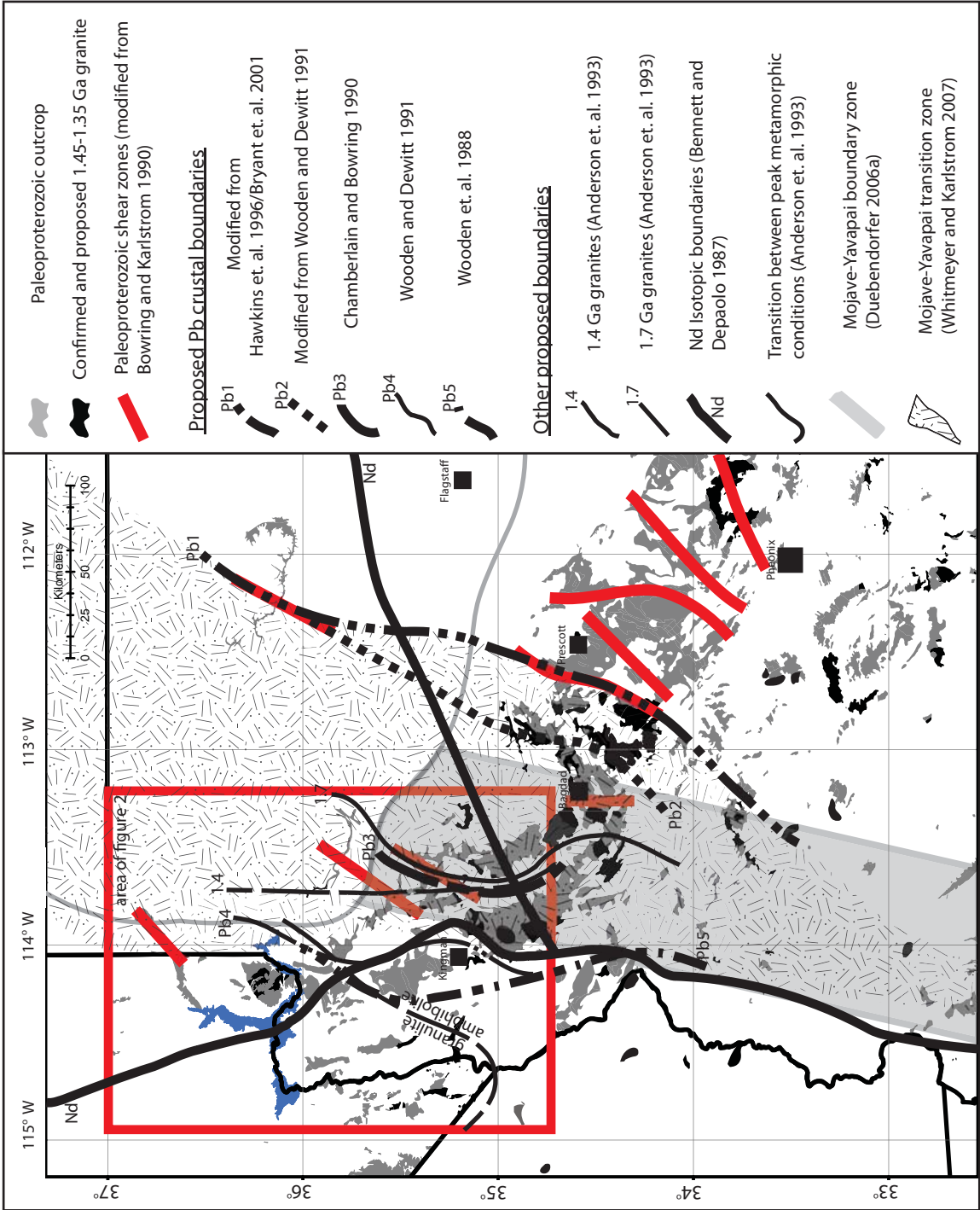
LIST OF TABLES

<i>Table 1. Lower Granite Gorge D_3 fabric orientations and overall sense of shear.....</i>	<i>12</i>
<i>Table 2. Quartz deformation temperature estimates for laboratory and naturally deformed samples</i>	<i>18</i>
<i>Table 3. Assembled $^{40}\text{Ar}/^{39}\text{Ar}$ ages for the Lower Granite Gorge, Virgin Mountains, and in the Gold Butte block near the Great Unconformity.....</i>	<i>32</i>

INTRODUCTION AND REGIONAL BACKGROUND

The Precambrian basement of the southwestern U.S. was formed during a complex series of tectonic events, starting with crust formation, dominantly in the Paleoproterozoic, followed by a major tectonomagmatic event in the Mesoproterozoic. These events produced a highly heterogeneous and segmented basement that influenced later Phanerozoic tectonic events, including modern deformation (Karlstrom and Humphreys 1998). The Proterozoic rocks exposed in northwestern Arizona and southeastern Nevada (figure 1) provide an excellent field laboratory for understanding accretionary crustal assembly and subsequent tectonism. Important structures of this region include pervasive north-east trending high strain zones separating blocks with different chemical and metamorphic characteristics, and thermal histories (Karlstrom et. al, 1987, figure 1). This study focuses on a broad transitional boundary located in NW Arizona between the Mojave and Yavapai Proterozoic crustal provinces (Karlstrom and Bowring 1991, Whitmeyer and Karlstrom 2007, Duebendorfer et. al. 2006a). These provinces are characterized primarily by difference in Pb and Nd isotopic signatures, which suggest greater influence by Archean crust in the Mojave province relative to the isotopically juvenile Yavapai province to the east (Bennett and DePaolo 1987, Wooden and Dewitt 1991). The larger Archean influence in the Mojave province may suggest the presence of Archean crust and mantle in the subsurface (Lee and Rudnick 2001, Whitmeyer and Karlstrom 2007). Differences in granitoid geochemistry, and metamorphic conditions have also been observed between provinces (Irriondo et. al. 2004, and references therein). Because of the complexity of rocks exposed in the region, the exact nature, location, and trend of this boundary zone has been the topic of numerous

Figure 1. Proterozoic outcrop and proposed Paleoproterozoic crustal boundaries in northwestern Arizona—based on locations of high strain zones, and isotopic, geochemical, and metamorphic changes observed. Base map for this figure and figure 2 compiled using data from Ferguson et al. (2004), Reynolds (1988), Twichell and Cross (2003), USGS (2005).



papers (Karlstrom and Bowring 1988, Bowring and Karlstrom 1990, Karlstrom et. al. 2003, Duebendorfer et. al. 2006a, Bickford and Hill 2007, Whitmeyer and Karlstrom 2007). Thus, a better understanding of deformational history in this region is important for constraining crust formation history of southern Laurentia and its relationship to Proterozoic and older cratons (see Schufeldt et.al. 2010, Ramo and Calzia 1998).

The oldest exposed Paleoproterozoic rocks consist of 1840 Ma arc-related plutonic rocks of the Elves Chasm Gneiss (Ilg et. al. 1996), which forms the basement for supracrustal volcanic and pelitic sequences, ranging in age from ~1750 - ~1730 Ma. These are in turn cross-cut by ~ 1700-1660 Ma intrusive rocks (Karlstrom and Bowring 1993), that often have A-type chemistry (Anderson et. al. 1993), and are interpreted to reflect melting of lower crust due to tectonic over thickening (Karlstrom et. al. 2003). Mesoproterozoic plutonic rocks in the region, depicted in figure 1, are commonly A-type megacrystic granites that range in age from 1450-1350 Ma, and are now recognized to be associated with significant regional deformation and metamorphism, where strain was enhanced in thermally softened pluton aureoles (Nyman et. al. 1994, Ferguson et. al. 2004). Shaw et al. (2005) showed that crustal temperatures at this time were highest near pluton aureoles, but also reached temperatures of 300-500 °C regionally at depths of ca. 10 km, implying a combination of high geothermal gradients (30-45 C/km) and “regional contact” metamorphism (e.g. Collins et. al. 1991, Glazner et. al. 2004).

Peak metamorphic conditions in the region occurred between ~1700 Ma to ~1650 Ma (Anderson et. al. 1993, Karlstrom et al. 2003). In the Mojave province, high amphibolites and granulite conditions were reached, while in the Yavapai/Mojave transition zone, greenschist to upper amphibolites conditions were reached. Within the

Yavapai/Mojave transition zone, adjacent blocks experienced marked differences in peak metamorphic conditions over a relatively short wavelength. For example, the Hualapai Mountain block reached conditions between 580 and 650 °C at pressures of 200-250 MPa, while the Cottonwood cliffs block to the east experience lesser conditions (450-530 °C at 200-300 MPa) (Williams 1991). In western Grand Canyon, this is also observed, with the Spencer Canyon block exhibiting higher peak conditions of 650-750 °C and up to 650 MPa and the Travertine Grotto block recording 550-600 °C and 250-350 MPa, (Robinson 1994).

Previous thermochronologic work has shown that the region is similar to much of the southwestern USA in that most basement rocks cooled through 300-350 °C by about 1.4 Ga (Bryant et al 2001; Shaw et al., 2005, Flowers et. al. 2005), although some areas cooled through 300-350 °C earlier, and were colder than 300-350 °C at 1.4 Ga (Dumond et. al. 2003). This has been interpreted to mean that much of the basement terrane was in the middle crust (~10 km) at 1.4 Ga, which has been supported by thermobarometry done around several 1.4 plutons (Nyman et. al. 1994). Detailed studies in Arizona show that many rocks are characterized by slow (< 5 °C/Ma) cooling following ca 1.7 Ga peak metamorphism (Hodges et. al. 1994, Hodges and Bowring 1995, Chamberlain and Bowring 2001). The combined data suggest long term residence of rocks in the middle crust from 1.7- at least 1.4 Ga following convergent tectonism (Karlstrom and Williams 1995, Karlstrom and Williams 2006, Williams and Karlstrom 1996). Hotter peak metamorphic blocks initially cooled more slowly than colder blocks following peak metamorphism (referred to here as “hot” and “cold” blocks respectively) such that adjacent tectonic blocks exposed within the region show different early cooling paths

(Chamberlain and Bowring 2001, this paper). While the region as a whole cooled slowly after peak metamorphic conditions at ~1.7 Ga herein a “hot” crustal block is defined as one that exhibits relatively slower cooling from peak metamorphic conditions to Some possible explanations for very long-term (several 100 Ma) T-t difference in cooling histories between adjacent blocks has been proposed to be: 1) different heat generation character of blocks (Flowers et. al. 2004, 2005), 2) different degrees of reheating by 1.4 Ga magmatism and fluids (Nyman et. al. 1994, Dumond et. al. 2003), and 3) 1.4 movement on faults and shear zones to juxtapose different 1.4 Ga isotherms (Dumond et. al. 2003; this paper). Resolution of this issue is needed for better understanding of both thermal behavior in this region through time, and for understanding of the enigmatic 1.4 Ga tectonic-magmatic event in southwestern Laurentia.

Proterozoic deformational fabrics consist of NW-striking S_1 and NE-striking S_2 (figure 2). S_1 is folded but has enveloping surfaces that dip moderately NE. The S_2 fabric is NE trending and subvertical to steeply NW dipping. Northeast-trending shear zones are D_2 -related and separate crustal blocks of differing compositions, ages, metamorphic grades and/or thermal histories (Albin and Karlstrom 1991). Although most workers agree that this region contains the diffuse transitional province boundary between the Mojave and Yavapai provinces (Albin and Karlstrom 1991, Duebendorfer et. al. 2006a, Whitmeyer and Karlstrom 2007), discrete tectonic and isotopic boundaries have been more elusive to define. Figure 1 shows the location of proposed boundaries, which are based on changes in composition, isotopic values, metamorphic conditions, and coincidence of these with high strain shear zones.

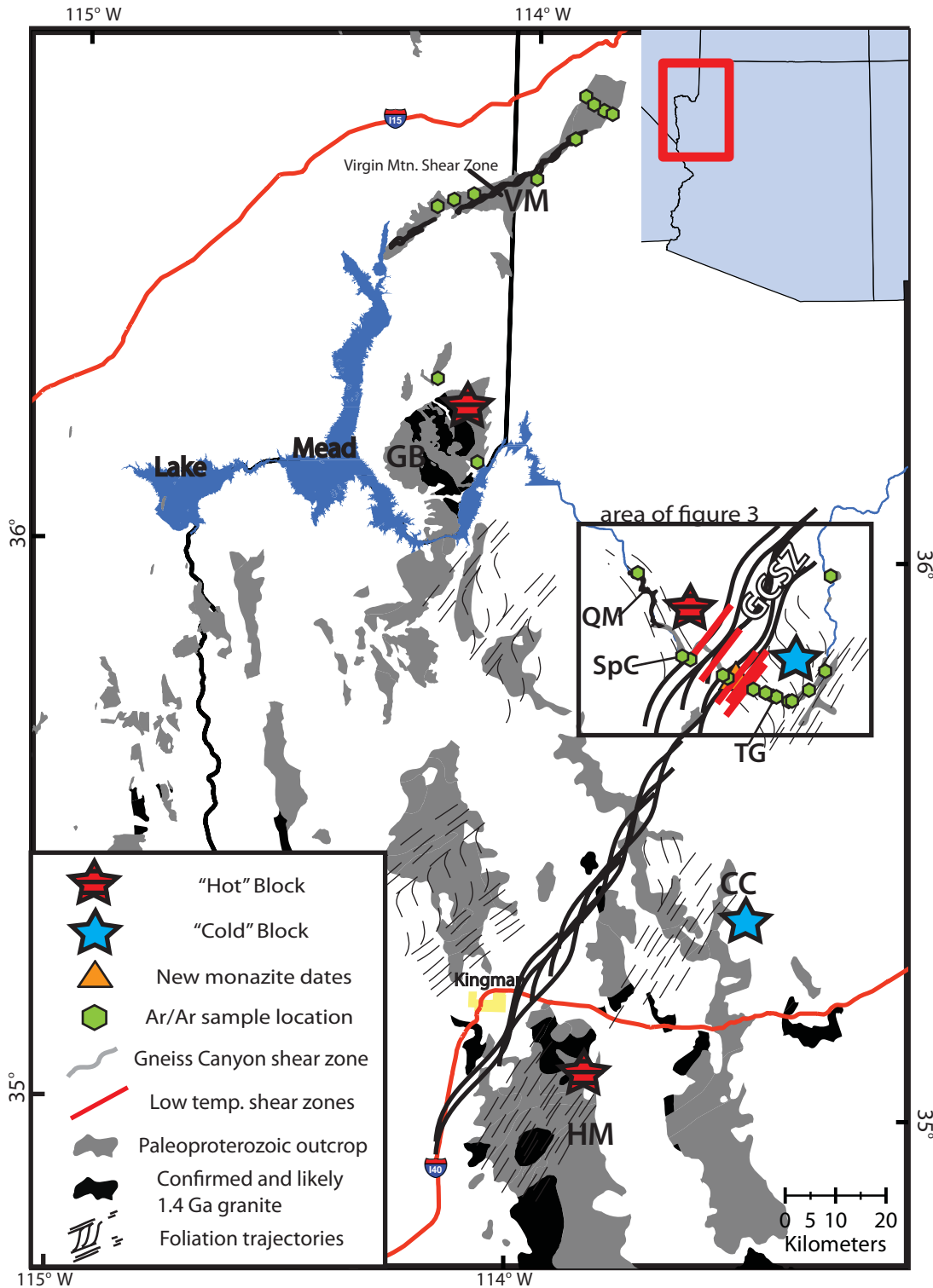


Figure 2. Geologic map of NW Arizona and SE Nevada showing Gneiss Canyon shear zone and distribution of Paleoproterozoic rocks and Mesoproterozoic plutons. CC = Cottonwood Canyon, GB = Gold Butte, GCSZ = Gneiss Canyon shear zone, HM = Hualapai Mtns., SpC = Spencer Canyon, QM = Quatermaster Granite, VM = Virgin Mountains (modified from Albin and Karlstrom 1991).

The Gneiss Canyon shear zone of western Grand Canyon is one such zone separating blocks with differing thermal histories (this study), metamorphic conditions (Robinson 1994) as well as a slight change in Pb–isotopic signature (Karlstrom et al., 2003 based on Wooden (unpublished)). This shear zone separates the lower grade Travertine Grotto block on the east from the higher grade Spencer Canyon block in western Grand Canyon (Robinson 1994). It is traceable southwest through the Grand Wash cliffs, Peacock Mountains and northern Hualapai Mountains (Albin, 1991; Albin and Karlstrom 1991) (see figure 2). The primary goal of this study is to incorporate new $^{40}\text{Ar}/^{39}\text{Ar}$ thermochronologic data and U-Th-Pb microprobe monazite ages, with new microstructural information and existing regional cooling data into a model for post-peak metamorphism kinematic history for the Gneiss Canyon shear zone.

GEOLOGIC SETTING

The Lower Granite Gorge (LGG) of western Grand Canyon sits near the southwestern margin of the Colorado Plateau (figure 2), and provides a 50-km-long continuously exposed transect of the basement rocks across part of the transitional boundary zone between the Mojave and Yavapai crustal provinces. Lithologies exposed in the Lower Granite gorge are largely correlative with units described above. Style and timing of deformation and metamorphism, are similar to rocks of the Upper, and Middle Granite gorge transects, which is summarized in Ilg et. al. (1996), Hawkins et. al. (1996), Karlstrom et. al. (2003), and Dumond (2007). Recent detrital zircon studies indicate the Vishnu Schist has similar detrital zircon populations across the entire Grand Canyon transect, including samples from the Lower Granite Gorge, and hence is likely from a

single correlative sedimentary succession (Shufeldt et al., 2010). 3) arc-related calc-alkaline plutons 1.75-1.71 Ga, interpreted to be shallow level arc plutons that were cogenetic with the arc supracrustal rocks, 4) peraluminous plutons of 1.7-1.66 Ga interpreted to be from collision-related melting of lower crust during continental assembly. 5) The 1.375 Ga Quartermaster pluton, interpreted to be part of regional intracontinental magmatism and related deformation that affected wide regions of the southwest. 6) Mesoproterozoic diabase dikes and sills described in Timmons et. al. (2005), which are interpreted to represent extension due to Grenville tectonism.

Figure 3 shows a geologic map of the Lower Granite Gorge. Supracrustal rocks include: 1) mafic Brahma schists- exposed intermittently in Diamond Creek, Granite Springs and Peach Springs canyons and from RM 228-237 (RM denotes river mile downstream from Lee's Ferry (Stevens 1983)), 2) felsic Rahma exposed in Peach Springs Canyon intermittently in Diamond Creek canyon and from RM 228 to 236 volcanic schists, and 3) pelitic schists and metaturbidites of the Vishnu Schist- exposed in Diamond Creek, Travertine Grotto (RM 229) and Spencer canyons near RM 234 and RM 236 (Karlstrom et. al. 2003) Vishnu schists provide good index minerals for metamorphic analysis at RM 229 and 246 (Robinson 1994). The oldest intrusive rocks exposed in the Lower Granite Gorge, exposed in the eastern part of the transect and near RM 245, are the 1.73 Ga Diamond Creek Pluton (RM 215-228 and Diamond Creek side canyon), its likely cumulate residue in Granite Park (RM207.5-208.5), and the 1.73 Ga granodiorite called the 245-mile granite (Karlstrom et. al. 2003).

Younger, synorogenic plutons are also voluminous in the Lower Granite Gorge. They include the 1704 ± 1 Ma Travertine Falls pluton (RM 230-231), Separation Pluton

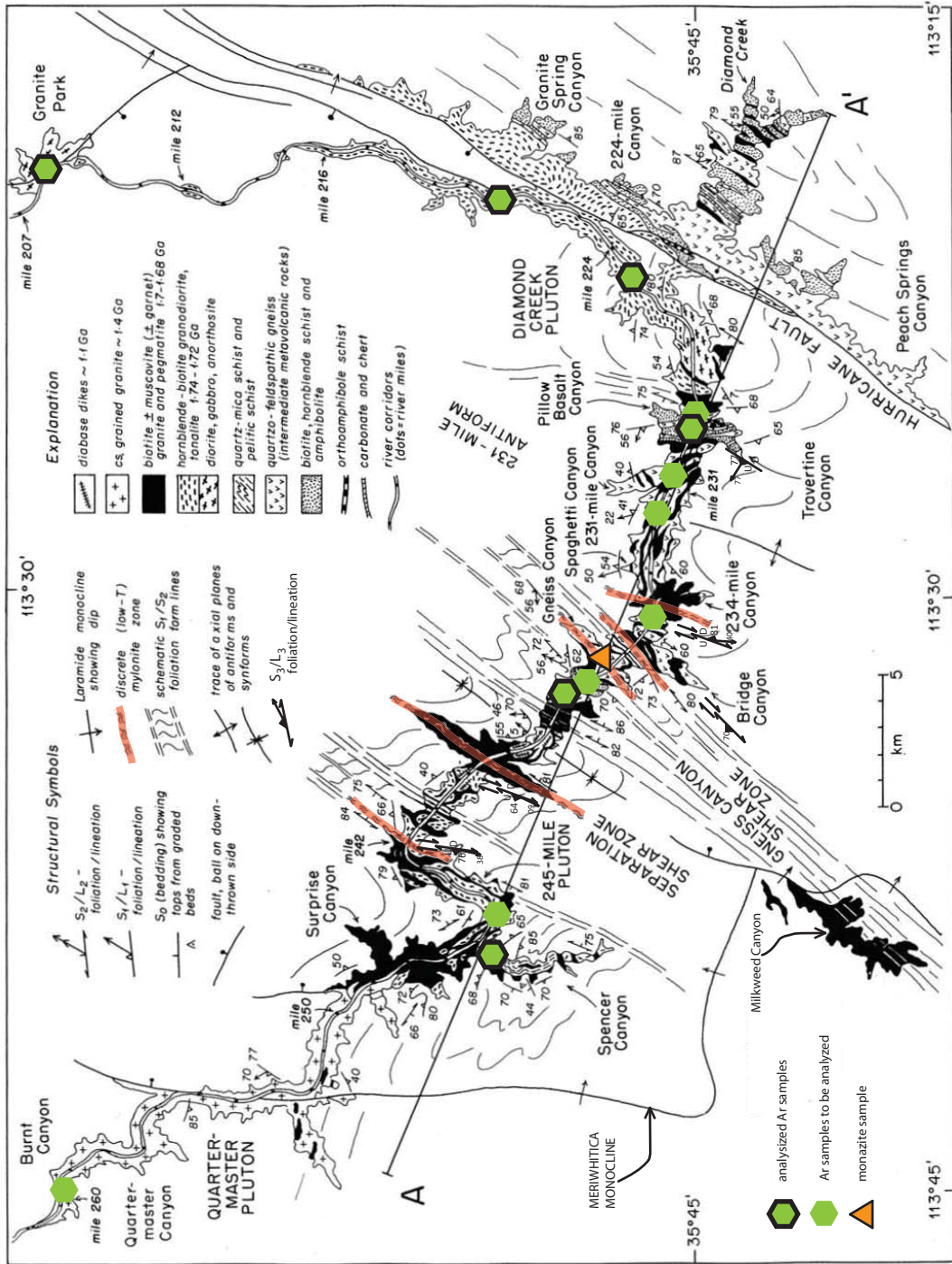


Figure 3 Geologic sketch map of Proterozoic rocks of the Lower Granite gorge with $^{40}\text{Ar}/^{39}\text{Ar}$ and monazite sample locations, see figure 4 for sample location key (modified from Karlstrom et.al. 2003).

(RM 239.3-239.8), 1678-1676 Ma Spencer pluton (RM 242-245) and 1690-1680 Ma Surprise Pluton (RM 246-252); these are interpreted to be collision-related crustal melts with ages between ~1700-1680 Ma based on metamorphic data (Karlstrom et.al. 2003, Bowring unpublished data). Their field geometry consists of complex intrusion networks of sills and dikes near the margins of stock-sized granite masses. The undeformed 1.375 Ga Quartermaster pluton (Bowring unpublished data) (RM255.5-RM261) is the youngest known plutonic body in the Lower Granite Gorge.

Rocks exposed along the transect are comprised of on the order of 40% granites, with Brahma, Vishnu, and Rama schist making of the balance of what is exposed. Figure 4 depicts these units as well sample locations in cross sectional view and shows the extent of crustal blocks in the Lower Granite gorge as they are discussed here. Table 1 shows D_3 Fabric orientations and sense of shear for oriented samples taken from the GCSZ.

Figure 5 shows field photos from western Grand Canyon which document primary depositional features as well as D_1 and D_2 ductile deformation. Primary depositional features can be seen Pillow-basalt canyon in the form of attenuated and chemically altered basalt pillow structures (figure 5d, long edge of photo is ~30 cm). S_1 fabrics are spectacularly exposed in Spaghetti canyon, where high magma pressure is documented by the presence of both ductile (figure 5a), and brittle (figure 5b) interactions of syntectonic granite dikes of probable 1700-1680 Ma age (Karlstrom et.al. 2003). This S_1 complex fabric is then rotated and intensified into steeply dipping D_2 high strain domains, which thus contain composite of the total D_1 - D_2 strain histories. Figure 5c shows a view looking northeast of steeply dipping S_2 foliation in pelitic (Vishnu) schist

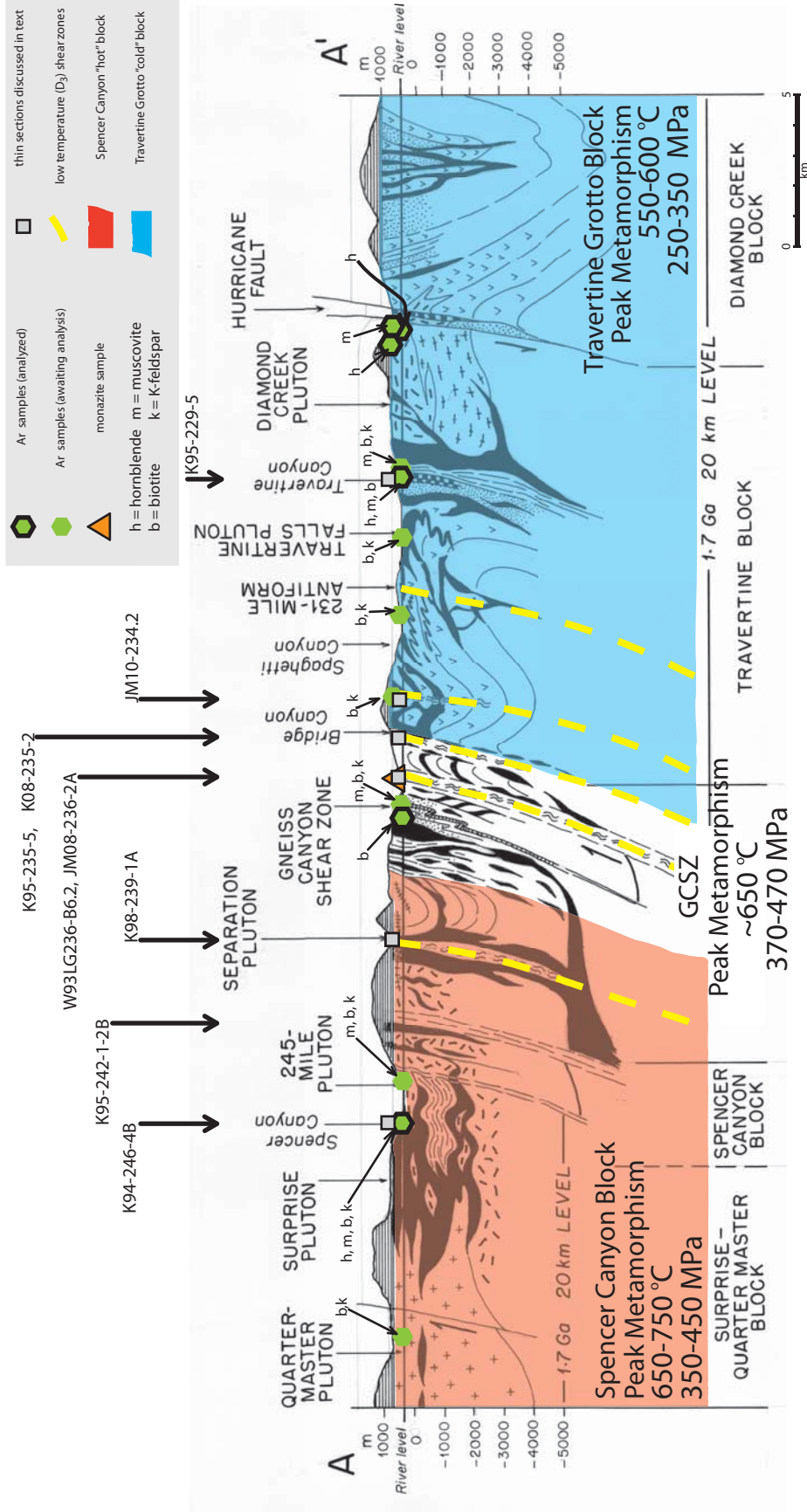


Figure 4. Schematic cross-section of Lower Granite Gorge transect A-A' --modified from Karlstrom et. al. 2003, Note dominance of steeply west dipping S_2 fabric. As discussed in the text, observed S_1 foliation generally strikes to the northwest and is shallow dipping. For lithologic symbols see figure 3. Metamorphic data from Robinson (1994).

Table 1. D_3 fabric orientations

sample	K95-229-5	JM10-234A	K94-235-2	K95-235-5	K98-239-1	K95 242.1-2B
river mile	229	234	235	235	239	242
foliation	032, 77W	020, 81E	045, 70W	020, vert.	020, 64W	008, 76W
trend and plunge lineation	down dip	40--->184	horizontal	horizontal	09--->205	38--->192
shear sense						

(base of photo is roughly 6 meters). High temperatures during D_2 are illustrated in figure 5f, which shows a plan-view composite photo of a folded, and boudinaged mafic dike from 245-mile canyon with pen and Brunton for scale pointing north. Granites participated in deformation during D_1 and D_2 as shown by migmatites in both S_2 (Figure 5 e) and S_1 .

As shown in Figs. 3 and 4, the roughly 13 km wide, north-east trending Proterozoic Gneiss Canyon shear zone is located near the center of the 50 km basement transect (RM 234–242.2) in the Lower Granite Gorge of Grand Canyon, AZ (Karlstrom et. al. 2003). Pb isotopic data (Wooden unpublished) as well as change in metamorphic conditions, and the occurrence of a ~10 m wide lens of carbonate located at RM 236.5 led Karlstrom et. al. 2003 to hypothesize that Gneiss Canyon shear zone may represent a Proterozoic crustal suture. However, the relative homogeneity of the detrital zircon signature of the Vishnu schist across the entire Grand Canyon transect, (Schufeldt et. al. 2010) suggest that if there is a significant crustal suture at either the Crystal or Gneiss Canyon shear zones, it likely formed prior to deposition of the Vishnu Schist ca. 1740 Ma. So as with the Crystal shear zone, if the Gneiss Canyon shear zone shear zone is the locus of a Paleoproterozoic suture, then shear during peak conditions ~1690 Ma may be due to reactivation of existing (D_1) planes of weakness.

Rocks exposed east of Gneiss Canyon shear zone exhibit peak metamorphic conditions of 550-600 °C and 250-350 MPa, whereas rocks exposed on the west side of Gneiss Canyon shear zone exhibit peak condition of 650-750 °C and 350-650 MPa (Robinson, 1994). The current tectonic model (Karlstrom et. al. 2003) is for west-up thrusting of west side over east, heating (from syntectonic plutons and regional

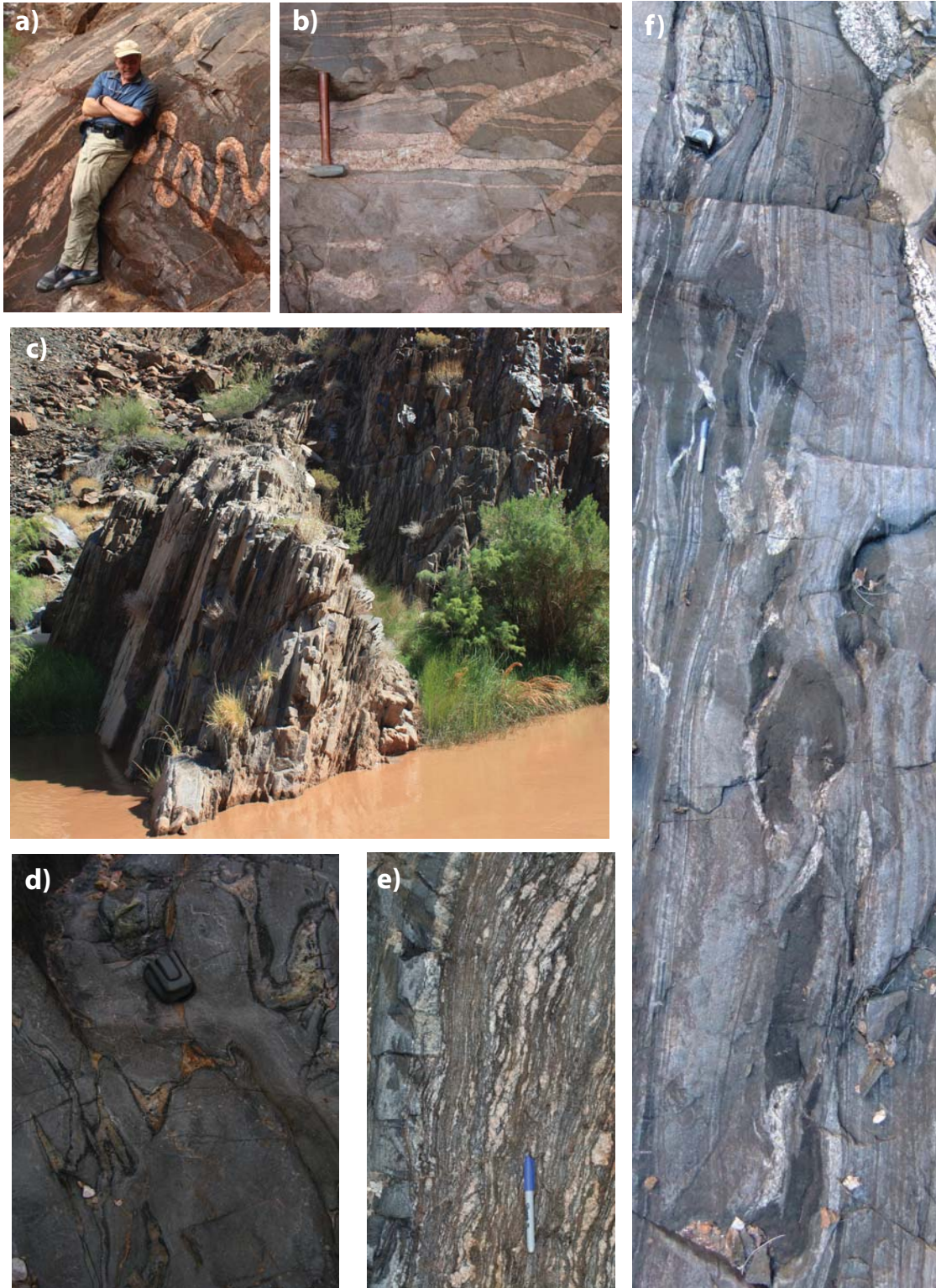


Figure 5. Field photographs of D_1 fabrics in Spaghetti Canyon and high temperature D_2 fabrics elsewhere in western Grand Canyon. See text for discussion. Photos (a,b,d) courtesy of Ryan Crow, (c) courtesy of Laura Crossey.

metamorphism) and decompressing of west side as the east side was being heated and compressed. This interpretation is consistent with structural mapping and thin section work (Albin, 1991, Albin and Karlstrom, 1991, Robinson, 1994, Hutchison, 1996). Microstructural evidence, presented here, shows similar sense of shear in several discrete 1 to 5-meter-wide, lower-temperature (< 500 °C) mylonite zones within the wider, high temperature (> 500 °C), Gneiss Canyon shear zone.

Thus, Spencer Canyon and Travertine Grotto have looping P-T paths of different sizes, which are interpreted to be broadly synchronous at about 1.69-1.68 Ga, based on field relations with dated plutonic rocks (Albin and Karlstrom 1991, Karlstrom et. al. 2003). Timing of deformation and metamorphism east of the shear zone is constrained by a 1698 Ma date on metamorphic sphene and 1670 ⁴⁰Ar-³⁹Ar age on hornblende, the latter of which gives the time of cooling through about 500 °C. West of the shear zone, U-Pb monazite dates on syntectonic and cross cutting granites range from 1700-1678 Ma and bracket deformation to that time interval (Karlstrom et al., 2003). Both sides of the shear zone have been thought to have been at the same depths of ~300 MPa after about 1670 Ma such that total unroofing of both blocks between peak metamorphic conditions and formation of the Great Unconformity was about 10 km. The geothermal gradient during the end of peak metamorphism may have been on the order of ~45 °C/km (Robinson 1994). Under this model, assuming a geobaric gradient of 30 MPa/ km, the differences in pressure of 300 versus up to 470 MPa corresponds to an maximum inferred throw of >5 km across the shear zone during and following peak metamorphic conditions. A dextral strike-slip component is suspected because of the oblique westerly rake of lineations seen in NE striking planes, but the extent of strike slip is unknown.

STRUCTURAL GEOLOGY

Methods

Structural observations in the basement rocks of the Lower Gorge show 2-3 generations of ductile deformation fabric, which is named here based on the nomenclature of Hobbs et. al. (1976). The earliest deformation fabric S_1 is preserved locally in apparent low strain zones and porphyroblast; it strikes northwest and has a shallow to moderate dip to the southwest (Albin and Karlstrom 1991, Hutchison 1994, Karlstrom et. al. 2003). Dates for this deformation have been constrained via field relationships to be pre-1.700 Ma (Karlstrom et. al. 2003) (see figure 5 a, b, d, f, and figure 6 a-c). This generation of fabric locally has more than one generation of folds (e.g. F_{1a} , F_{1b}), etc. and Ilg et. al. (1996) referred to these as group 1 rather than using the F_1 designation for this group of folds and fabrics which reflect earliest, initially sub-recumbent, probably thrust related progressive deformation.

In much of the Lower Granite gorge, this foliation is overprinted by a second, locally more pervasive, set of steeply dipping fabrics (D_2). Foliations associated with this deformation are northeast-trending with steep southwest-to-near-vertical dips (figure 5 c), (Hutchison 1994, figure 6 a-c). High temperature shear in the Gneiss Canyon shear zone is included with this generation of fabrics and includes locally abundant migmatites and high temperature shear zones. As outlined above, timing of this second fabric formation was between 1700 Ma and ~1650 Ma, after peak metamorphism in Spencer canyon, and synchronous with peak metamorphic conditions in Gneiss Canyon shear zone and Travertine Grotto as discussed earlier (Hutchison 1996, Karlstrom et.al. 2003, this study).

A third (D_3 or late D_2), fabric is shown in low temperature mylonite shear zones referred to as D_3 here (after Karlstrom et. al. 2003). These cm-to-m scale lower temperature zones are characterized by apparent intensification of grain size reduction relative to surrounding material (figure 7) with occasional pseudotachylite. They tend to occur within felsic plutonic rocks, predominantly within the eastern portion of the Gneiss Canyon shear zone, RM 229, 231, 234, 234.2, and 235, but are also observed at river mile 242 (see figure 3 and 4). Orientations of these shear zones are generally coincident with, or slightly oblique to D_2 foliation. Timing of this generation may be as early as ~1650 Ma to as late as post 1400 Ma plutonism (see discussion below). Displacement is dextral and west-side-up.

Oriented samples from Gneiss Canyon shear zone, including these D_3 low temperature mylonite zones, were analyzed for sense of shear using shear sense indicators viewed on kinematic sections cut parallel to stretching lineation and perpendicular to the NE trending S_2 foliation, as outlined in Vernon (2004) and references within. Observed shear sense indicators include S-C fabrics, sigma and delta porphyroclasts, and offset grains. These were analyzed using techniques described in Lister and Snoke (1984), Simpson and Depaor (1993), Passchier and Trouw (1996). Microstructural analysis of D_2 and D_3 fabrics consistently show west-side-up shear, with a dextral component where lineations are not down dip.

Quartz and feldspar deformation microstructures were compared with experimental results (Hirth and Tullis 1992, Tullis et. al. 2000, Tullis 2002) and field studies (Dunlap et. al. 1997, Stockhert et. al 1999, Zulauf 2001, Stipp et. al. 2002) to gain qualitative estimates of temperatures during production of the various microstructures

<i>Zulauf 2001</i>	<i>Hirth & Tullis 1992</i>	<i>Stipp et. al. 2002</i>
pressure variable	1500 MPa	250-300 MPa
temperature <300 - >600 °C	500 - 1200 °C	250 - 700 °C
deformation rate $10^{-13} - 10^{-15}$ s	$10^{-6} - 10^{-5}$ s	$10^{-14} - 10^{-11}$ s
~300 C Cataclastic	Cataclastic	Cataclastic
lower greenschist facies level	Regime 1	BLG I
~500 C upper greenschist facies level	Regime 2	BLG II
~570 C amphibolite facies level	Regime 3	SGR
		GBM I
		GBM II
		280±20°C
		400±30°C
		= 500±30°C

Table 2. Comparison of quartz deformation temperature estimates for laboratory and naturally deformed samples. Comparison of quartz deformation temperatures estimates from naturally deformed samples with dislocation creep regimes of Hirth and Tullis 1992. Temperature estimates based on syntectonic metamorphic reactions (Stipp et. al. 2002, Zulauf 2001), and 40Ar/39Ar cooling ages from mica (Zulauf 2001).

(See table 2). Assuming normal orogenic deformation rates of 10^{-14} and 10^{-11} /second (Stipp et. al. 2002), observed microstructures indicate deformation at temperatures ranging from >500 °C to < 300 C. The higher T microstructures include core and mantle structure in feldspar, dynamically recrystallized rounded feldspar grains. Lower temperature (< 300 °C) microstructures included grain boundary migration recrystallization and core and mantle structure in quartz, deformation bands and undulose extinction in quartz, and undulose and fractured quartz and feldspar grains. This wide range of inferred temperatures may have formed in a single progressive event as rocks cooled from >650 to <300 °C after the Yavapai orogeny. However, the combined data sets (plutonic history, microstructures, $^{40}\text{Ar}/^{39}\text{Ar}$ and monazite) suggest a polyphase fabric forming history. In the following section, microstructural analysis is used to argue that low temperature microstructures are later and overprint high temperature microstructures within the D_3 retrograde shear zones. The local presence of altered psuedotachylite in some localities suggests that deformation took place near the brittle ductile transition and/or that strain rate may have been high towards the end of D_3 .

High temperature history of Lower Granite Gorge

Although metamorphic P-T thermobarometry studies give more info on P-T conditions (Robinson 1994; Dumond et al., 2007) and porphyroblast-matrix studies can inform interpretations of the timing of deformation (Hutchison 1996), deformational microstructures are focused on. High temperature microstructures for the Travertine Grotto block, the Gneiss Canyon shear zone, and Spencer Canyon block are shown in figure 6. Within the Travertine Grotto block, microstructures are largely dominated by

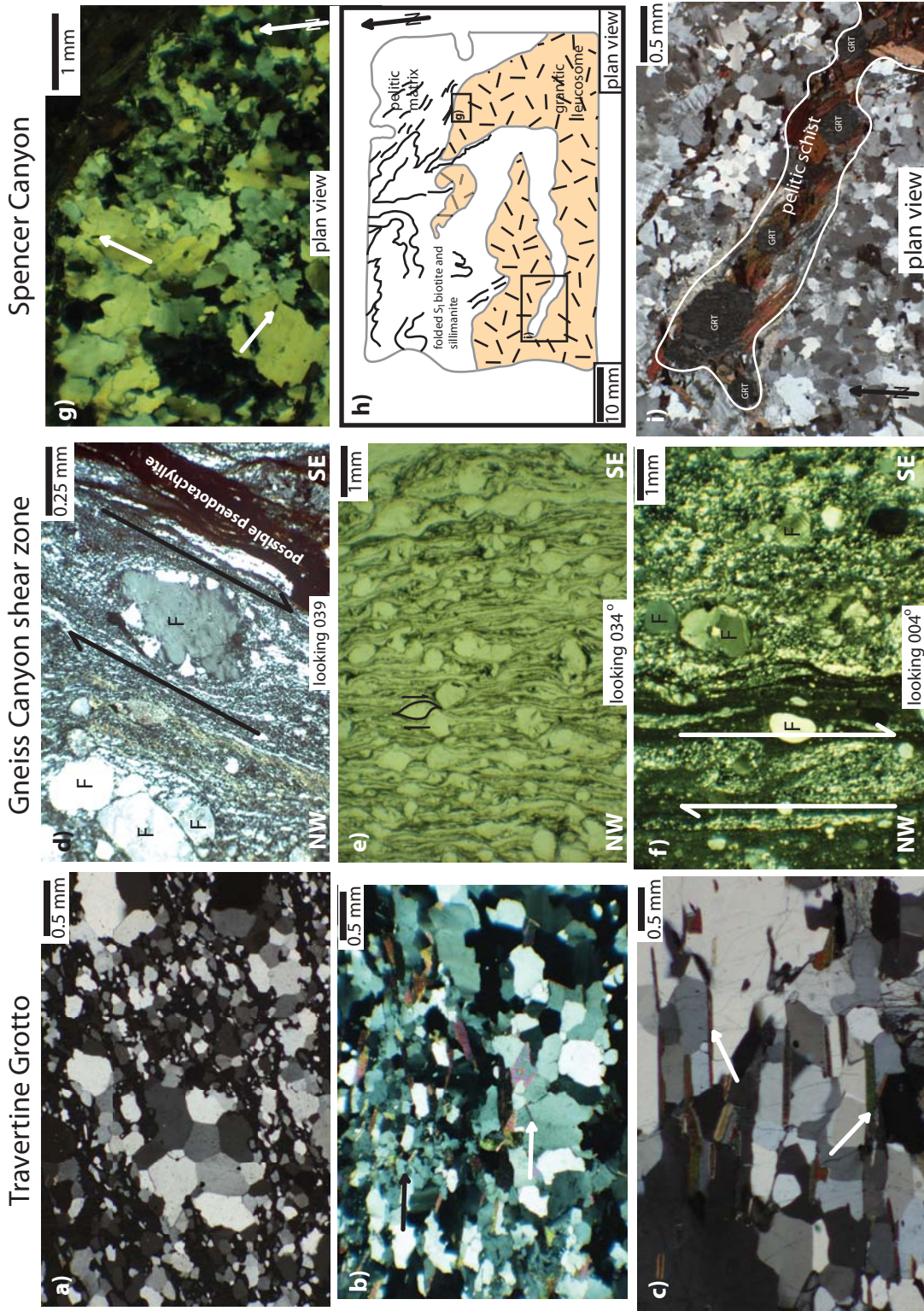


Figure 6. High temperature microstructures observed in Spencer Canyon and Travertine Grotto blocks, as well as Gneiss Canyon shear zone. See text for discussion.

quartz recovery under regime 3 of Hirth and Tullis (1992). For example, sample K 299-1 (figure 6 a) exhibits annealing in quartz, showing euhedral grains with 120 degree triple junctions and strong lattice preferred orientation in pure quartz domains which are interstitial to inclusion free garnet (black). In domains where accessory minerals are present, grain size and shape are commonly dictated by pinning at accessory mineral (commonly biotite, and feldspar) grain boundaries. Figure 6 b (also sample K 229-1) shows domains of smaller grains in the presence of accessory minerals (black arrow). 6 b and c (sample K95-229-8) shows pinning of quartz grain boundaries at accessory contacts (white arrows). These finer grained domains and the occurrence of grain boundary pinning is comparable with the grain boundary migration mechanism of dynamic recrystallization, (GBM I) as described by Stipp et. al. 2002, and suggests temperatures above 500 °C, agreeing with peak metamorphic condition calculated by Robinson (1994), and broadly agree with Hutchison (1996) that observed D₂ deformation was largely synchronous with late peak conditions.

Spencer Canyon sample K94-246-4B (figure 6 g-i) also exhibits high temperature quartz and feldspar microstructures, which are developed in leucosomes representing granitic partial melts at temperatures ≥ 650 °C (Robinson 1994, Hutchison 1996) (figure 6 h) during peak metamorphic conditions. Folding of biotite and sillimanite, as well as leucosomes (F₂ or F_{1b}), suggest that latter stages of metamorphism were likely synchronous with D₂ deformation. Quartz microstructures in granite within leucosomes include, irregular quartz grains with long axes that overgrow accessory biotite (GBM II of Stipp et. al. 2002) (figure 6 g white arrows), as well as grains with boundaries pinned to these accessory biotite (GBM I of Stipp et. al. 2002) (figure 6 i white arrows),. These

structures which indicate temperatures between ~ 560 and 650 °C, as well as inclusion free garnet (figure 6 i), indicate higher peak conditions than in the GCSZ and Travertine Grotto during, and suggest continued high temperatures after peak metamorphism and leucosome formation, during development of D₂ features.

Higher strain occurring in GCSZ rocks result in a more varied suite of textures, which also contain indicators of high temperature (>500 °C). These include migmatites zones described in Robinson (1994) that locally make up ~50% of country rock, as well as mylonites, characterized in the field by marked apparent grain size reduction, and the occurrence of mm-to-cm scale rounded feldspar grains (popcorn feldspar (see figure 6e, sample K08-235-2) in a dark brown or gray matrix. Under magnification, this matrix is predominantly comprised of biotite, quartz, and feldspar (see figure 6 f).

Rounded feldspars like these were interpreted by Tullis and Yund (1985) to be result of dynamic recrystallization of feldspar grains via continuous bulging recrystallization (similar to quartz BLG I of Stipp et. al. 2002, and regime 1 of Hirth and Tullis 1992) resulting in small subgrains at grain margins which are weaker than parent grains due to a relative lack of dislocations. Due to this relative weakness, these new grains take up most of the strain and are translated away from the parent grain during shear which leaves a rounded core with little evidence of internal strain. Feldspar begins to undergo dynamic recrystallization above ~500 °C, but compositional variance within individual grains may drive the temperature requirements down (Tullis et.al. 2000).

Higher temperature quartz microtextures are preserved locally, but are largely absent due to late overprinting by lower temperature features. Examples of overprinting are seen in figure 6f (sample JM10 234.2A) where a tight asymmetrically folded quartz ribbon

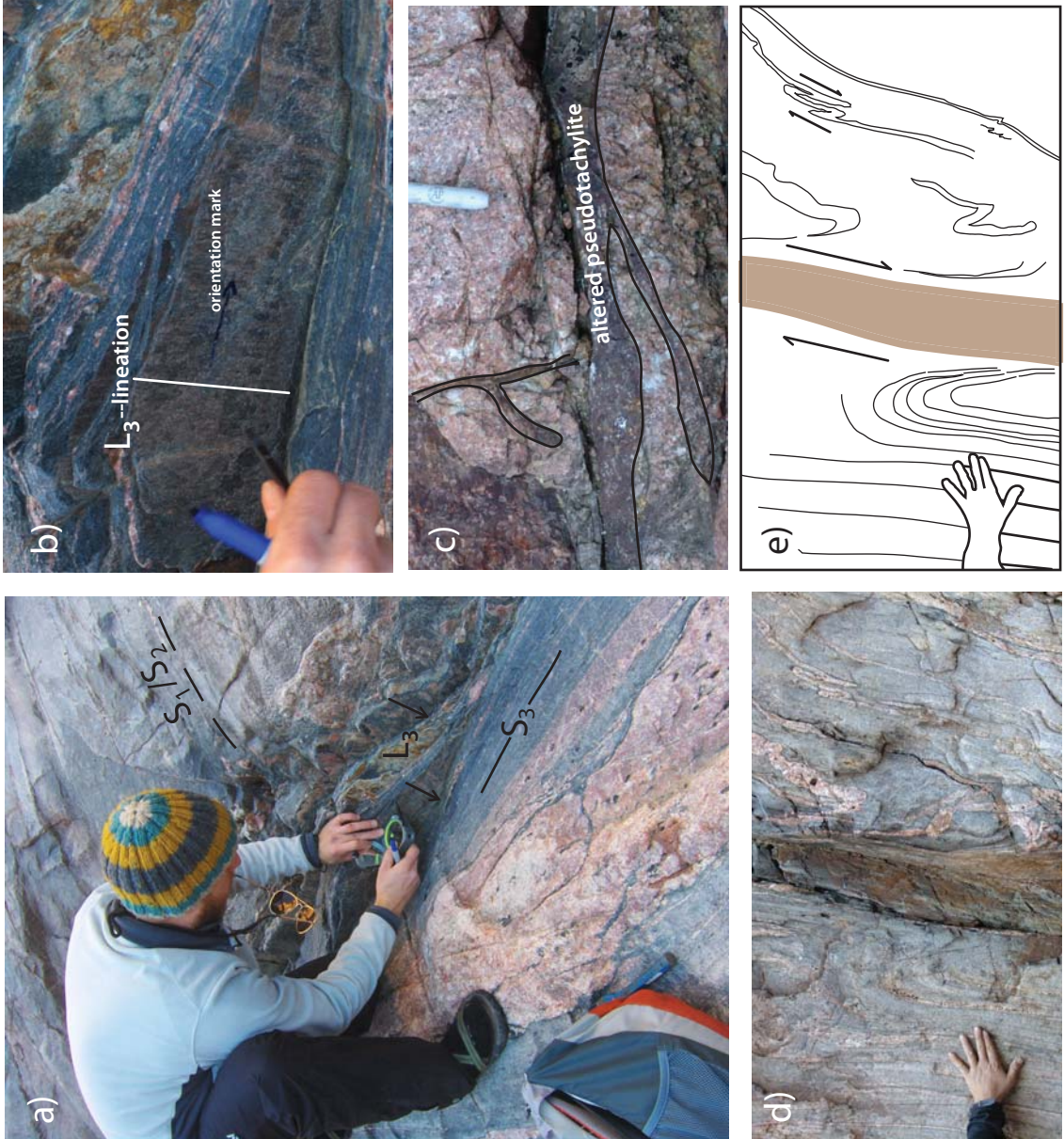
remain while quartz grains within this ribbon exhibit regime 2 deformation characteristics. Both vergence of the folds, and s-c fabric displayed within the ribbon indicate west-side-up sense of shear. Overprinting by lower temperature microstructures can also be seen in figure 6d (sample JM08-236-2a), where rounded feldspar are fractured (top left), “swimming” in regime 2 quartz (center), and cross cut by possible pseudotachylite (bottom right). Assuming normal deformation rates, microstructures observed in D₂ mylonites within the GCSZ indicate that deformation took place at temperatures >500 °C, with later overprinting at lower temperatures in the range ~450-~300 °C.

Low temperature shear zones and their microstructures

Microstructural evidence, presented here, shows similar west-side-up and dextral sense of shear in these lower temperature (< 500 °C) mylonite zones within the wider, high temperature (> 500 °C), Gneiss Canyon shear zone, though with perhaps greater strike slip component (see table 1, figure 8). Lower temperature samples show remnants of some of the higher temperature features mentioned above, but also show increased grain size reduction of feldspar via brittle cracking and features that suggest regime 2 and 1 deformation of quartz. Temperature estimates based on these textures are between ~450 °C and < 300 °C.

Samples taken from near river level and within side canyons at RM 229, 231, 234, 234.2, 235, 236, 239 and 242 (see figure 3) analyzed for this study show a consistent west-side-up and/or dextral sense of shear within D₂ and D₃ fabrics in Gneiss Canyon shear zone across a temperature range from >500 °C to ~300 °C. In many samples,

Figure 7. Field Photos of Low temperature (D_3) mylonites from RM 242: a) view to the southwest b) close up view of same location, note rounded feldspar, c) pen for scale points north d) and e) low temperature shear zone further downstream from a-c, view to the northeast hand for scale, note west-side-up shear sense indicated by deflection of gneissic foliation. See text for discussion. Photos a and b courtesy Molly Wick.



higher temperature (feldspar regime 1 and regime 2) deformation textures are overprinted by lower temperature (quartz regime 2) textures (figure 8 a-c, figure 6 d-f). The consistent shear sense observed in these samples indicates that both higher and lower temperatures occurred during contraction and west-side-up simple shear.

From analysis of microtextures alone it is difficult to tell whether strain accumulated during a single progressive event that may have spanned cooling from 500 to below 300 °C after the Yavapai orogeny, or whether the lower temperature microstructures reflects a later deformational episode. Many of the low temperature D₃ fabrics display a larger strike-slip component, which may indicate a progressive shift in principle strain axis orientations or strain partitioning during a single event, or it may indicate a rotation of principle strain axes as a result of a second deformation event.

As seen in the larger GCSZ, (see figure 6) many samples from lower retrograde shear zones exhibit a combination of higher and lower temperature textures. For example, figure 8 a (JM08-236-2A) and c (K95-235-5), both photos crossed polar view, shows well developed s-c fabric in grain size reduced low temperature quartz indicating west-side-up shear at Gneiss Canyon. Relic high temperature rounded feldspar (feldspar regime 1) temperatures are overprinted to quartz regime 2 temperatures. Figure 8 b shows brittle cracking of dynamically recrystallized feldspar adjacent to dynamically recrystallized quartz, an apparent drop from ~450 °C to below 300 °C (sample JM10-234B, crossed poles). Figure 8 d shows fracture array and antithetic “books” both indicate dextral brittle displacement of ductilely deformed quartz and feldspar (sample K98-239-1A, uncrossed nicols). Figure 8 e and f, both sample K95-242.1-2B show dextral displacement. Figure 8 e shows elongated ribbon quartz, with subgrains of

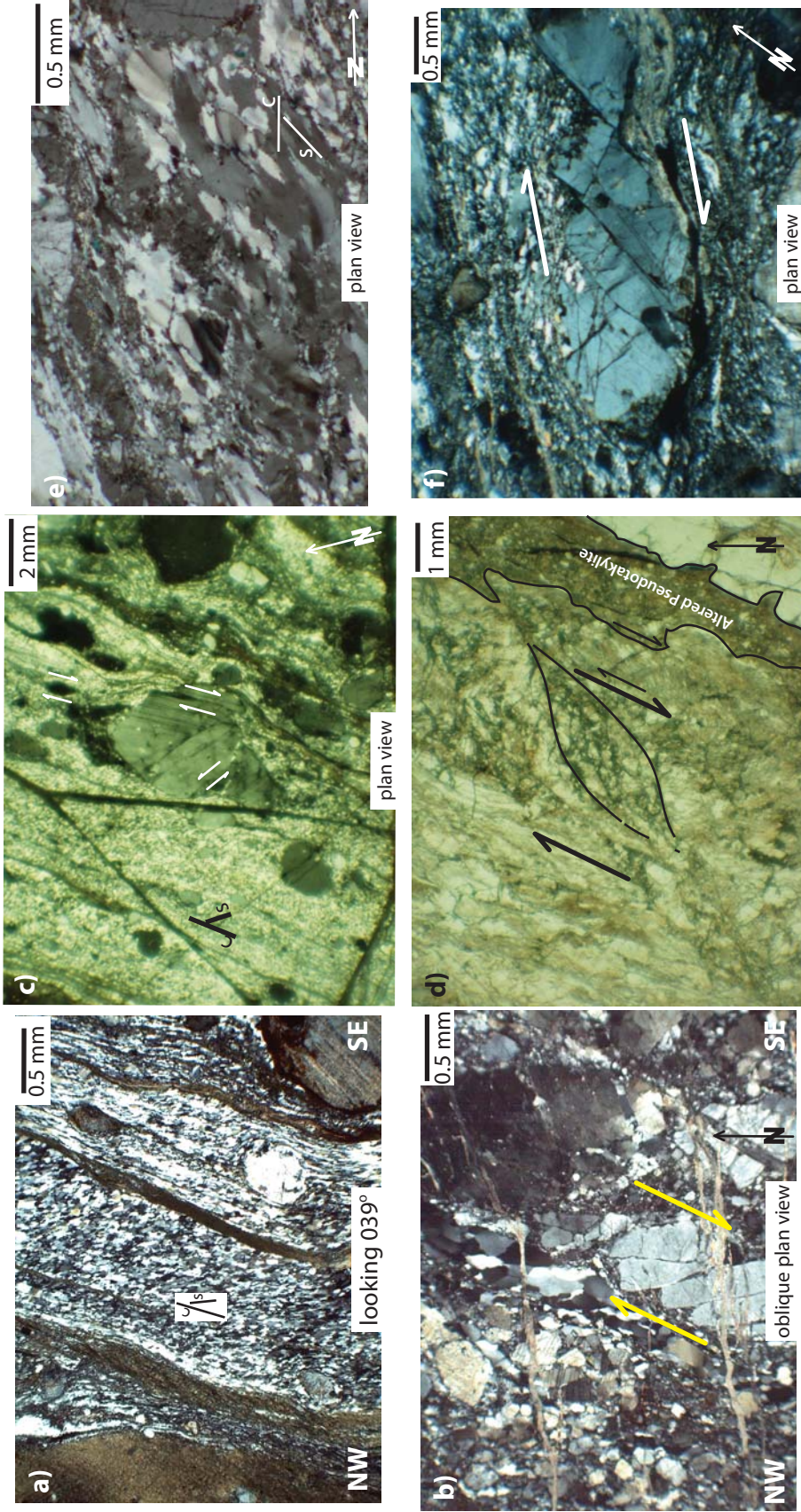


Figure 8. Select photomicrographs of low-temperature retrograde shear zones found within the Gneiss Canyon shear zone. See text for discussion.

similar size as newly formed grains indicating deformation in regime 2 ductile deformation of quartz. Figure 8 f shows a brittlely deformed K-feldspar grain with antithetic shear along fracture planes.

U-TH-PB MONAZITE DATING

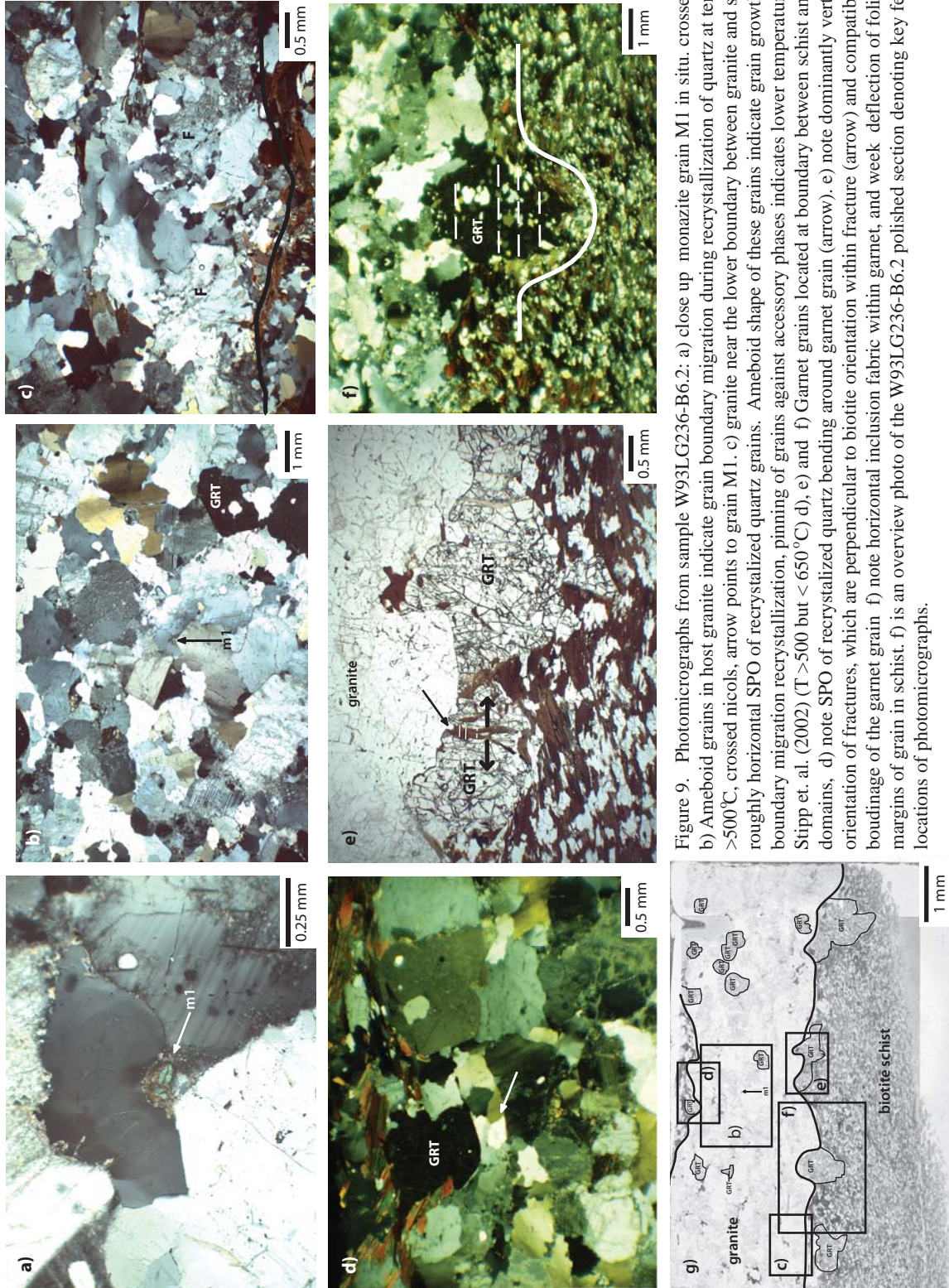
Methods and results

In situ electron microprobe analysis of sample W93LG236-B6.2 was conducted as described in Williams et. al. (2007) and references therein at the University of Massachusetts in Amherst. Electron microprobe analysis allows simultaneous compositional mapping and absolute dating of grains while allowing retention of context that can be observed in polished thin sections. Because diffusion within monazite grains is extremely slow, U-Th-Pb dates attained from domains as small as 5 μ m in width can be combined with textural context to learn absolute timing of deformational and metamorphic events (Williams et.al. 2007). Preliminary results are presented in figure 10 and show ages from 4 monazite grains analyzed from sample W93LG236-B6.2 with a total distribution ranging from > 1700 Ma to ~1600 Ma (figure 8a). Dates from a single grain (M1) shows growth of the core at 1696 \pm 14 Ma to 1648 \pm 16 Ma in the rims (figure 8b). Monazite can grow under a wide range of temperature conditions (Williams 2007), however ~1680-~1640 Ma hornblende Ar- Ar ages in the Travertine Grotto block and the ~1680 Ma granites in Spencer Canyon block are both consistent with temperatures above 500 °C during the period of monazite growth. Therefore, these ages likely reflect crystallization during emplacement of the host Y-rich granite dike at ~1696 Ma, followed

by later mobilization of fluids and growth at near peak metamorphic conditions associated with garnet growth within the dike during the Yavapai orogeny.

Microstructures of Monazite-dated sample

As described above, this sample (W93LG236-B6.2) gives a range of monazite ages that document progressive deformation from 1700-1630 Ma. Thus, deformation microstructures within this sample are important to provide age constraints on the high-T deformation fabrics. This sample also exhibits high temperature feldspar and quartz microstructures (see figure 9). W93LG236-B6.2 was taken from Gneiss Canyon at RM 236, and is comprised primarily of two domains, one is a biotite schist of the Vishnu schist and the other is a small (~0.5 cm) granitic dike or leucosome that intrudes the schist parallel with foliation. The sample does not show evidence for asymmetric fabrics indicative of simple shear in either the granite or schist. Fabrics are defined by alignment of elongated quartz grains and biotite within both schist and the margins of the granite vein. This S_1 foliation displays weak local crenulation (S_2 or S_3 ?) Garnet is found near the schist-granite margins and within the felsic dike. Within the schist, inclusion trails within garnet are comprised of biotite, and quartz \pm feldspar, and are generally parallel to sub-parallel to S_1 matrix foliation. S_3 crenulation formation may be post garnet growth as suggested by straight inclusion trails and bending of matrix against some garnet grains. Garnets within granite are relatively inclusion poor and are nearly devoid of biotite inclusions, again suggesting high temperature diffusional equilibration of the garnet. This suggests garnets here record higher temperatures in the dike relative the schist via increased re-equilibration by diffusion. Large embayments in some garnets near schist-



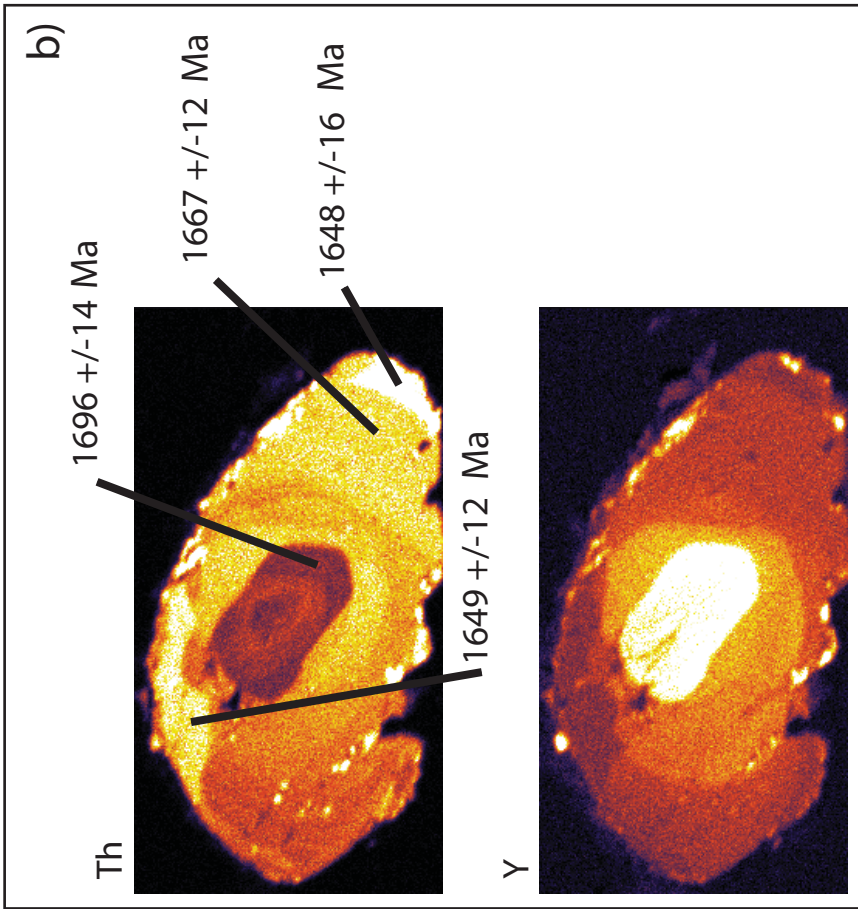
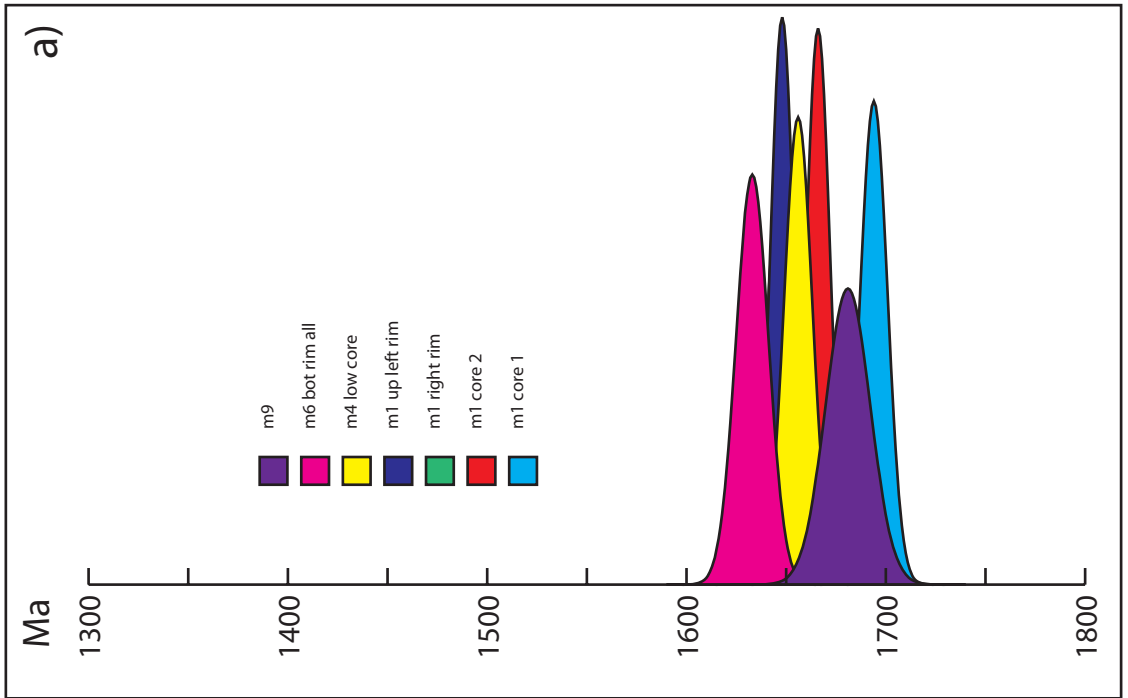


Figure 10. Monazite results from sample W93LG236-B6.2: a) Age probability plot of ages for analyzed monazite grains from W93LG236-B6.2 b) Th and Y maps of monazite M1 of sample W93LG236-B6.2 indicating distinct zoning with regards to both elements and ages of these zones with 2σ error. This grain is from the granite domain of the section (see 9 a and b). The age of the inner core is interpreted to represent a crystallization age of this granite leucosome/dike. Courtesy of Mike Williams (UMASS)

granite interface, coupled with nearby garnets within the granite, may suggest plucking of garnets during emplacement of dike (see figure 9 e)

These observations suggest a sequence beginning with foliation development in the schist during D₁, followed by crenulation development and some garnet growth before/during emplacement of the granite dike D₂. Later, high temperature, D₂ intensification of foliation is suggested by a domain of relatively strain free recrystallized quartz grains, which appear to bend around the one garnet (figure 9d), and by biotite alignment with schist foliation and schist-garnet interface, found in a fracture that is perpendicular to this foliation (figure 9 e, arrow). Because of the timing and temperature relationships discussed above, U-Pb monazite dates between ~ 1700 and ~1630 Ma from grains found in W93LG236-B6.2 (figure 10) are interpreted to record ~70 Ma of progressive D₂ deformation during peak and near peak metamorphic condition. Importantly, all microstructures are high temperature, such that there is no evidence for substantial cooling to below 500 °C during this time frame and instead, it is inferred that lower temperature microstructures observed in other areas represent a separate, post-1630 ma event.

⁴⁰AR/³⁹AR THERMOCHRONOLOGY

Methods

Samples for ⁴⁰Ar/³⁹Ar analysis were collected from localities with the Travertine Grotto and Spencer Canyon blocks, as well as from Gneiss Canyon shear zone, and from basement rocks exposed just beneath the Great Unconformity at Devil's Cove, in southeastern Nevada. Preparation of all samples for ⁴⁰Ar/³⁹Ar analysis included manual

Sample	location§	mineral	Plateau Analysis Age	$\pm 1\sigma$	TGA Age	$\pm 1\sigma$	source	Comments
H98-208-2	RM208†	hornblende	1712	2	1696	2	this study	
H225-4	RM225	hornblende	1638	3	1619	2	this study	
H225-5A	RM225	hornblende	N/A	N/A	1920	2	this study	
K93-225.5	RM225.5	hornblende	1701	4	1647	3	this study	
DC-25	RM229	hornblende	1680	3	1645	2	this study	
T02-221-1	RM222	muscovite	1564	2	1563	3	this study	
K94-229-2	RM229	muscovite	1559	3	1546	2	this study	
LG-229-3	RM229	muscovite	1576	3	1555	2	this study	
K94-229-2	RM229	biotite	1576	3	1532	2	this study	
LG-229-3	RM229	biotite	1528	3	1488	2	this study	
H225-5c	RM225	K-spar	N/A	N/A	1172	2	this study	MDD model
DC-236-6	RM236	hornblende	N/A	N/A	1431	3	this study	
AZ-349	~RM238	hornblende	1626	4	1595	1	this study	
K00238-2	238	hornblende	1638	2	1624	3	this study	
LG-237-1	RM237	biotite	1534	3	1526	2	this study	
AZ-349	RM238	biotite	N/A	N/A	1559	3	this study	
AZ-89-38	RM245	hornblende	1658	4	1601	2	this study	
DC-42	RM246	muscovite	1526	3	1497	1	this study	
DC-42	RM246	biotite	1401	3	1325	1	this study	
DC-42	RM246	K-spar	N/A	N/A	1298	3	this study	MDD model
KGB-99-16	Pig's ear	hornblende	1613	2	1571	2	Karlstrom et. al. 2010	
KGB-99-16	Pig's ear	biotite	1424	2	1412	2	Karlstrom et. al. 2010	
KGB-99-16	Pig's ear	K-spar	1346	5	1324	2	Karlstrom et. al. 2010	
K00GB-4	Devil's Cove	hornblende	N/A	N/A	1502	2	this study	
K00GB-5	Devil's Cove	hornblende	1656	3	1673	2	this study	
52-1-89	Gold Butte	muscovite	1374	13	1368	11.7	Reiners et. al. 2000	
K00GB-4	Devil's Cove	biotite	1371	2	1339	2	this study	
KGB99-1	Gold Butte	K-spar	1400-1200*	N/A	1214	2	Karlstrom et. al. 2010	MDD model
Q60B	Virgin Mountains	hornblende	1668	5	1571	5	Quigley 2002	
Q81	Virgin Mountains	hornblende	1638	17	2048	18	Quigley 2002	
Q90A	Virgin Mountains	hornblende	1630	35	1638	5	Quigley 2002	
Q12	Virgin Mountains	hornblende	1639	20	1628	5	Quigley 2002	
Q108	Virgin Mountains	hornblende	1524	52	1554	4	Quigley 2002	
Q119	Virgin Mountains	biotite	N/A	N/A	843	3	Quigley 2002	
Q60B	Virgin Mountains	biotite	1416	4	1279	4	Quigley 2002	
Q90A	Virgin Mountains	biotite	1511	4	1511	4	Quigley 2002	
Q81	Virgin Mountains	biotite	1375	15	1364	3	Quigley 2002	
QFT-18	Virgin Mountains	biotite	N/A	N/A	522	3	Quigley 2002	
QFT-20	Virgin Mountains	biotite	1336	33	1306	4	Quigley 2002	
QFT-21	Virgin Mountains	biotite	1351	49	1317	4	Quigley 2002	
QFT-14	Virgin Mountains	biotite	1365	18	1359	4	Quigley 2002	
QFT-24b	Virgin Mountains	biotite	1419	10	1408	4	Quigley 2002	
Q119	Virgin Mountains	K-spar	N/A	N/A	898	3	Quigley 2002	
Q45	Virgin Mountains	K-spar	N/A	N/A	1418	5	Quigley 2002	
Q95	Virgin Mountains	K-spar	N/A	N/A	1133	6	Quigley 2002	
QFT-10	Virgin Mountains	K-spar	N/A	N/A	1362	5	Quigley 2002	
QFT-14	Virgin Mountains	K-spar	N/A	N/A	1250	4	Quigley 2002	
QFT-18	Virgin Mountains	K-spar	N/A	N/A	1211	6	Quigley 2002	
QFT-20	Virgin Mountains	K-spar	N/A	N/A	1369	5	Quigley 2002	
QFT-21	Virgin Mountains	K-spar	N/A	N/A	1246	5	Quigley 2002	
QFT-24B	Virgin Mountains	K-spar	N/A	N/A	1120	4	Quigley 2002	

* interpreted from visual inspection of MDD model, † located east of the Hurricane fault, § Grand Canyon samples (RM) = river miles downstream from Lee's ferry.

mineral extraction and cleansing to provide monomineralic specimens. Analytic methods are presented in Sanders et. al. 2006. K-feldspar MDD analysis methodology is also presented in Sanders et. al. (2006), and Karlstrom et. al. (2010).

Results

Individual Ar-Ar spectra for analyses noted below are present in figures 11 (hornblende), 12 (muscovite), 13 (biotite), and are summarized in table 3 along with Ar-Ar results from previous studies done in northwestern Arizona and southeastern Nevada. The Travertine Grotto block cooled through 500 °C by ~1638 Ma, as shown by an Ar-Ar age on hornblende from the Diamond Creek pluton. Muscovite spectra show plateau ages ranging from 1573 to 1556 Ma, with a mean age of 1556 ±5 Ma. A similar total gas ages mean of 1555 ±4 Ma for muscovite is interpreted to indicate that the Travertine Grotto block cooled through about 350 °C by ~1555 Ma. Biotites from this block are similar in age to the muscovite and yielded plateau ages of 1576 ±3 and 1528 ±3 Ma (mean of 1552 ±4 Ma). Biotite Ar-Ar ages are interpreted to reflect the time of cooling through about 300 °C. However, one of the biotite samples is older than muscovites from the same block, which is interpreted to reflect variable Ar retentively, and hence a closure temperature for this grain similar to the muscovites. The combined data suggest that the Travertine Grotto block cooled from peak temperatures of ca. 550 °C at ~1700-1640 Ma to ambient conditions of 300-350 °C at ca. 10 km depth at a geotherm of 30-35 °C /km.

Three samples were analyzed from the eastern side of the Gneiss Canyon shear zone at river miles 237 and 238. These gave similar results to the eastern block. Hornblendes yielded a mean plateau age of 1632 ±5 Ma; biotite gave a plateau age of

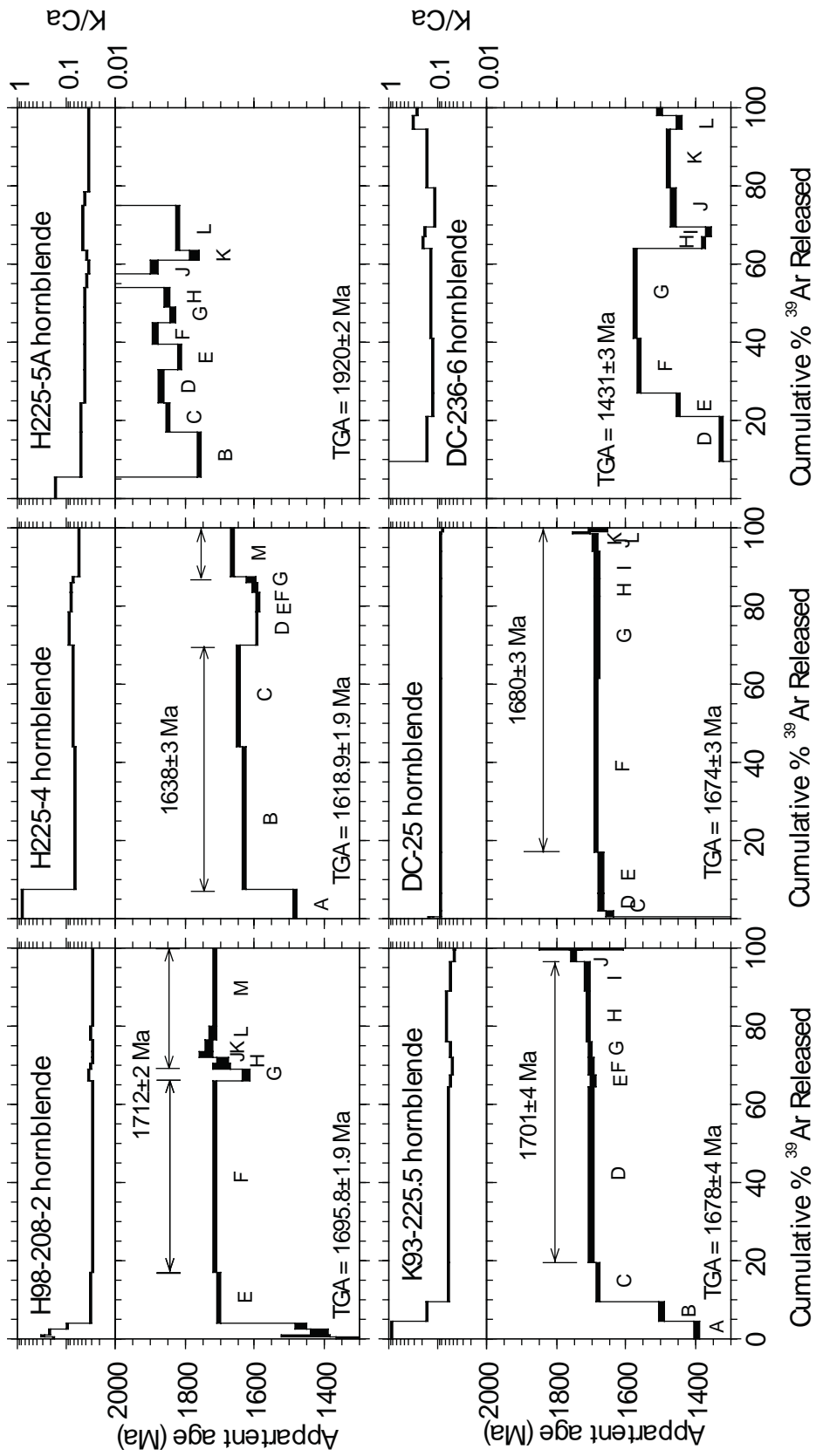


Figure 11. Hornblende $^{40}\text{Ar}/^{39}\text{Ar}$ spectra for the Lower Granite Gorge and Devil's Cove. Note that plateau ages range from 1712 ± 2 to 1626 ± 4 Ma suggesting cooling of the middle crust after assembly below $\sim 500^\circ\text{C}$ by this time. See table 3 for sample location in river miles below Lee's Ferry. Courtesy of Matt Heizler, NM Tech.

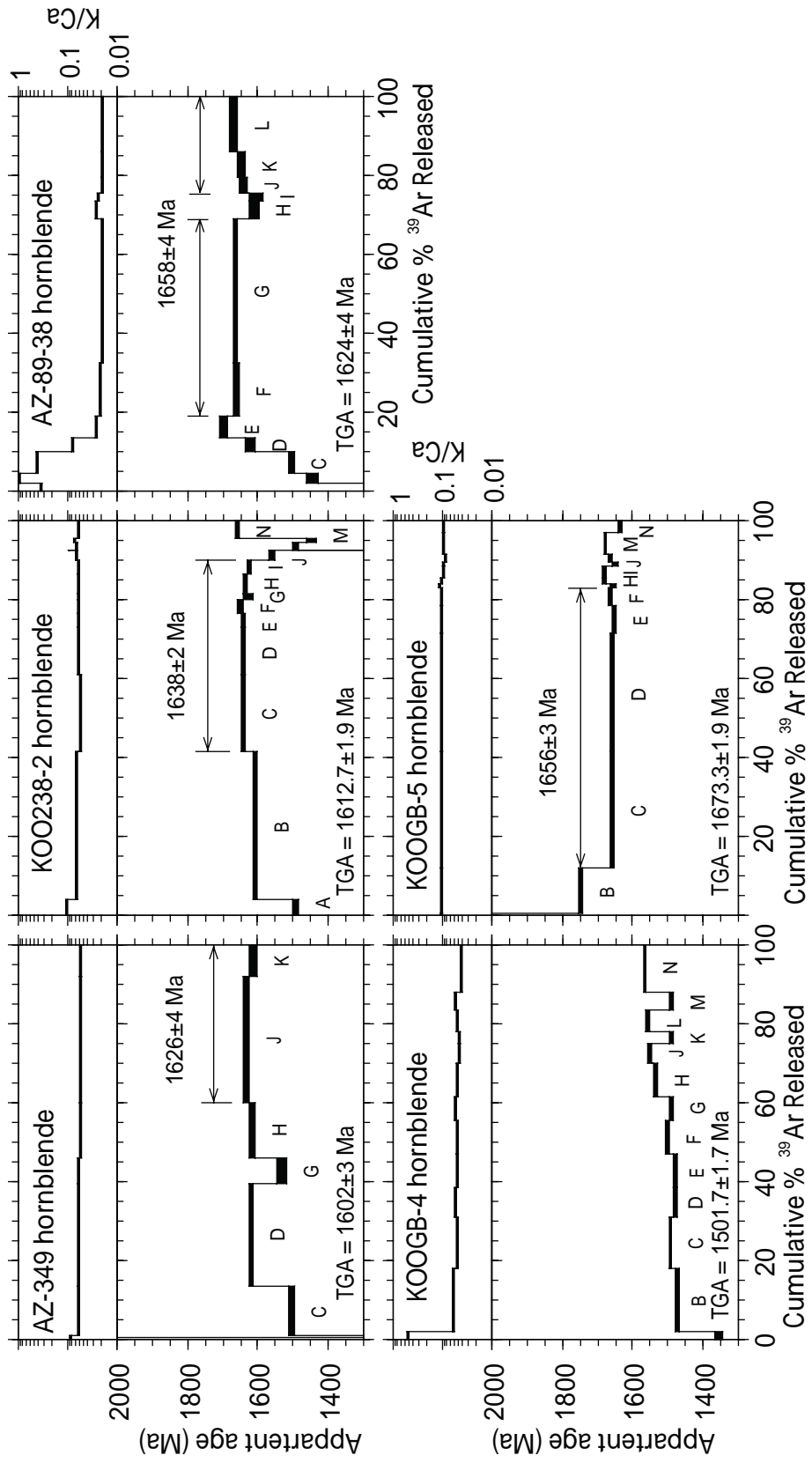


Figure 11 continued.

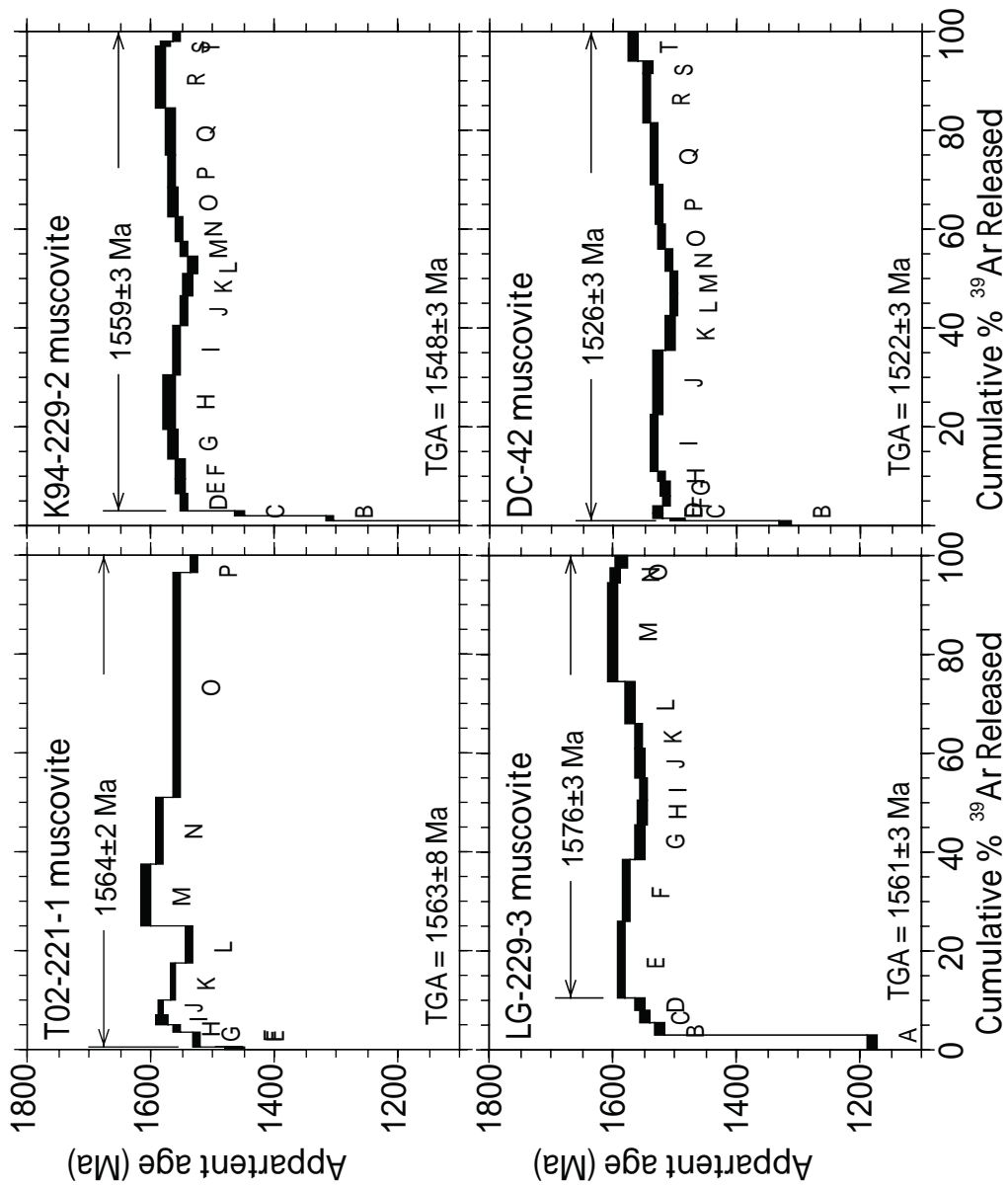


Figure 12. Muscovite $^{40}\text{Ar}/^{39}\text{Ar}$ spectra for the Lower Granite Gorge (Courtesy of Matt Heizler, NM Tech)

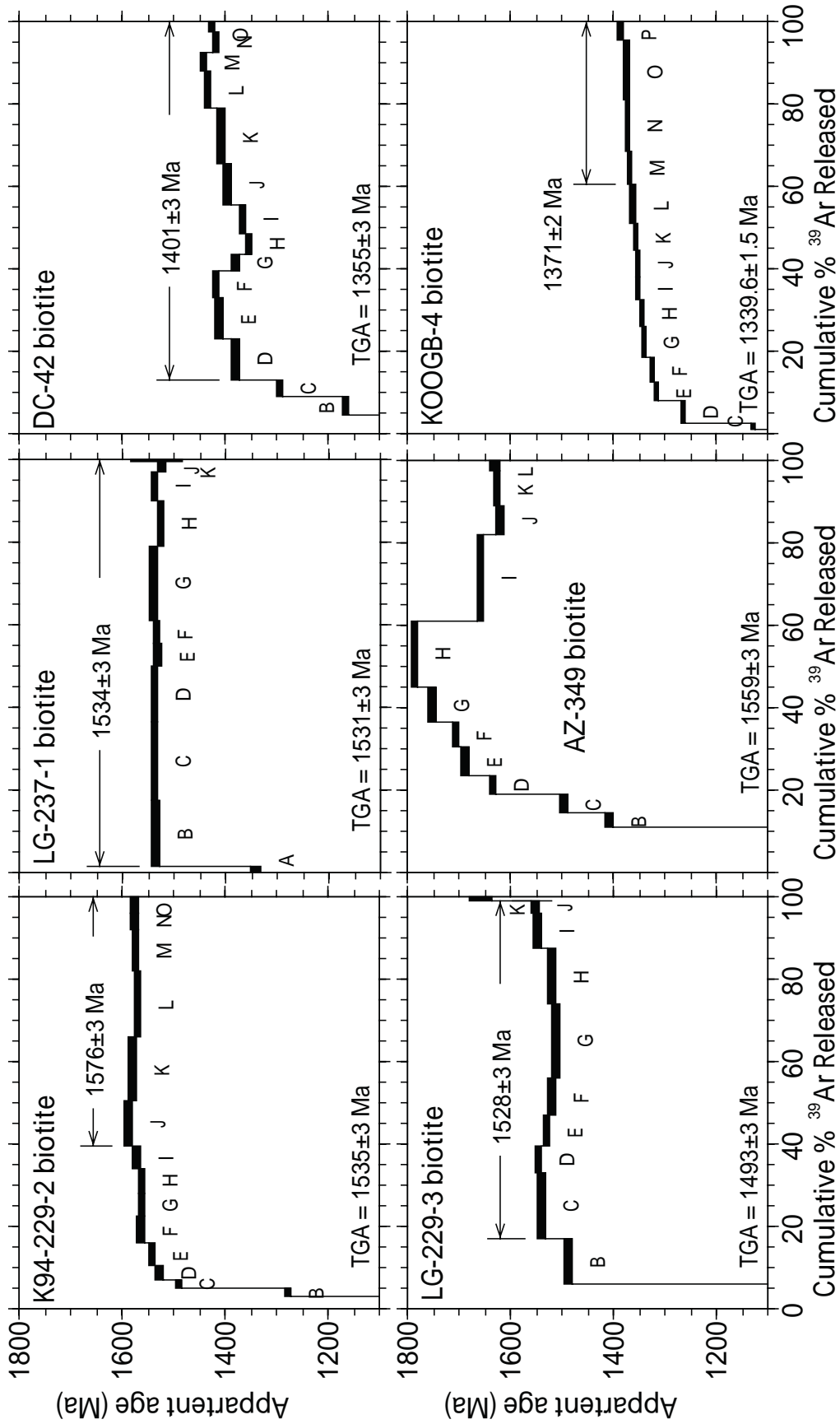


Figure 13. Biotite $^{40}\text{Ar}/^{39}\text{Ar}$ spectra for the Lower Granite Gorge and Devil's Cove (Courtesy of Matt Heizler, NM Tech).

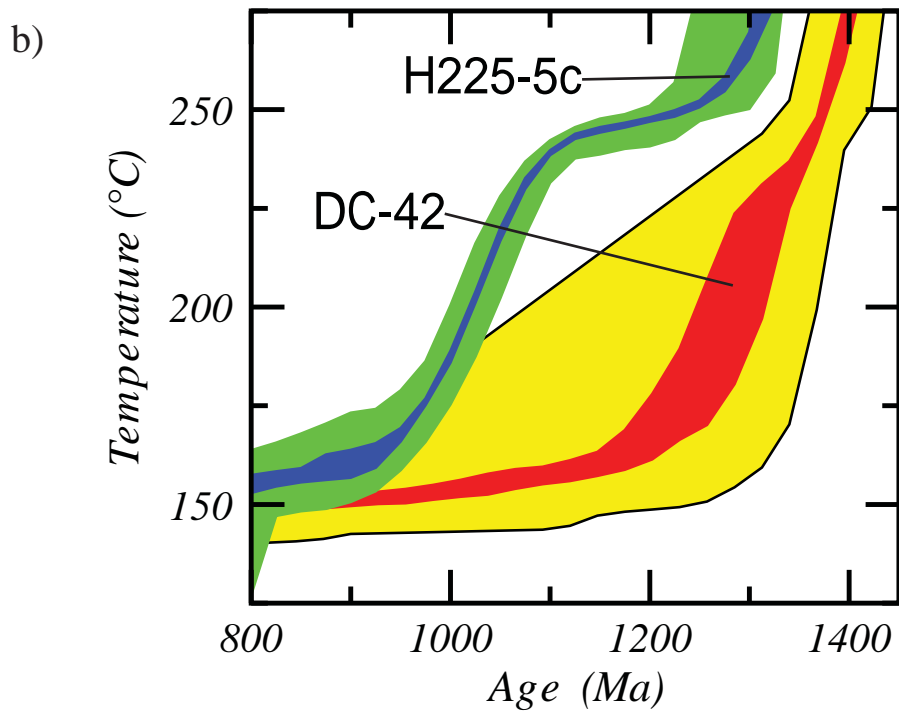
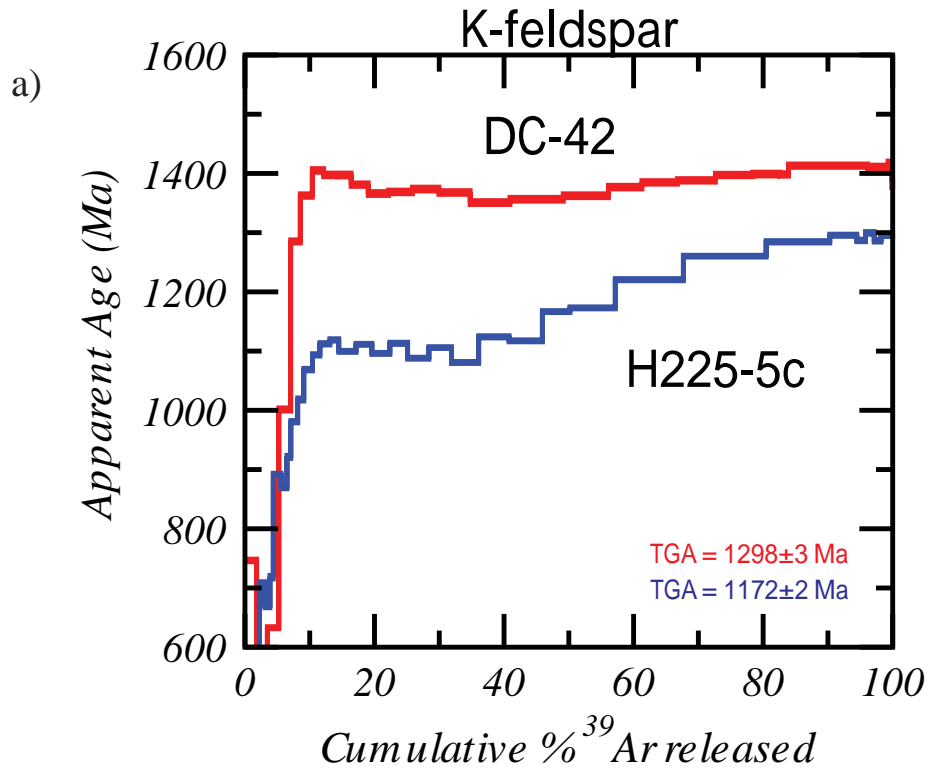


Figure 14. a) K-Feldspar $^{40}\text{Ar}/^{39}\text{Ar}$ spectra for the Lower Granite Gorge, b) MDD model plots for same samples indicating later cooling of travertine grotto block from $\sim 300^{\circ}\text{C}$ to $\sim 175^{\circ}\text{C}$ (Courtesy of Matt Heizler, NM Tech)

1534 ±3 Ma. These are interpreted to indicate cooling of the Gneiss Canyon blocks from 500 to 300 °C, somewhat later than cooling of the Travertine Grotto block.

Samples from the Spencer Canyon block give similar, results for hornblende (1658 ±4 Ma plateau age). Muscovite (1526 ±3 Ma) indicating cooling from 500-350 °C by ~1520 Ma. Biotite from Spencer Canyon area has saddle –type spectrum with a plateau age of ~1400 ±3 Ma and a total gas age of 1325 ±1 Ma.

Ar-Ar dates were also obtained from basement exposures that immediately underlie Cambrian strata in tilted fault blocks of the Basin and Range areas, just west of the mouth of Grand Canyon at Devil’s Cove. A hornblende age from Devil’s Cove closely matches the sample from Spencer Canyon, while the biotite age from this location gives an age of 1374 ±2 Ma ca. 30 Ma younger than a muscovite from Spencer Canyon.

Post- 1.4 Ga cooling history is recorded by low temperature, K-spar $^{40}\text{Ar}/^{39}\text{Ar}$ cooling ages and MDD modeling that offers the potential to give T-t paths as the rock cooled from 275 (most retentive domains in K-spar) to 175 °C (least retentive domains). Travertine Grotto block K-feldspar MDD analysis yield cooling from 275 °C at ~1300 Ma to 175 °C by ~900 Ma. MDD analysis of K-feldspar from the Spencer Canyon block indicate cooling from 275 °C at ~1400 to ~175 °C by ~1200 Ma, though the error estimates are higher for this analysis (figure 14).

DISCUSSION OF DIFFERENTIAL COOLING HISTORIES IN NORTHWESTERN ARIZONA

In order to gain a more complete regional cooling history data presented in this study are incorporated with thermochronologic data from northwestern Arizona and

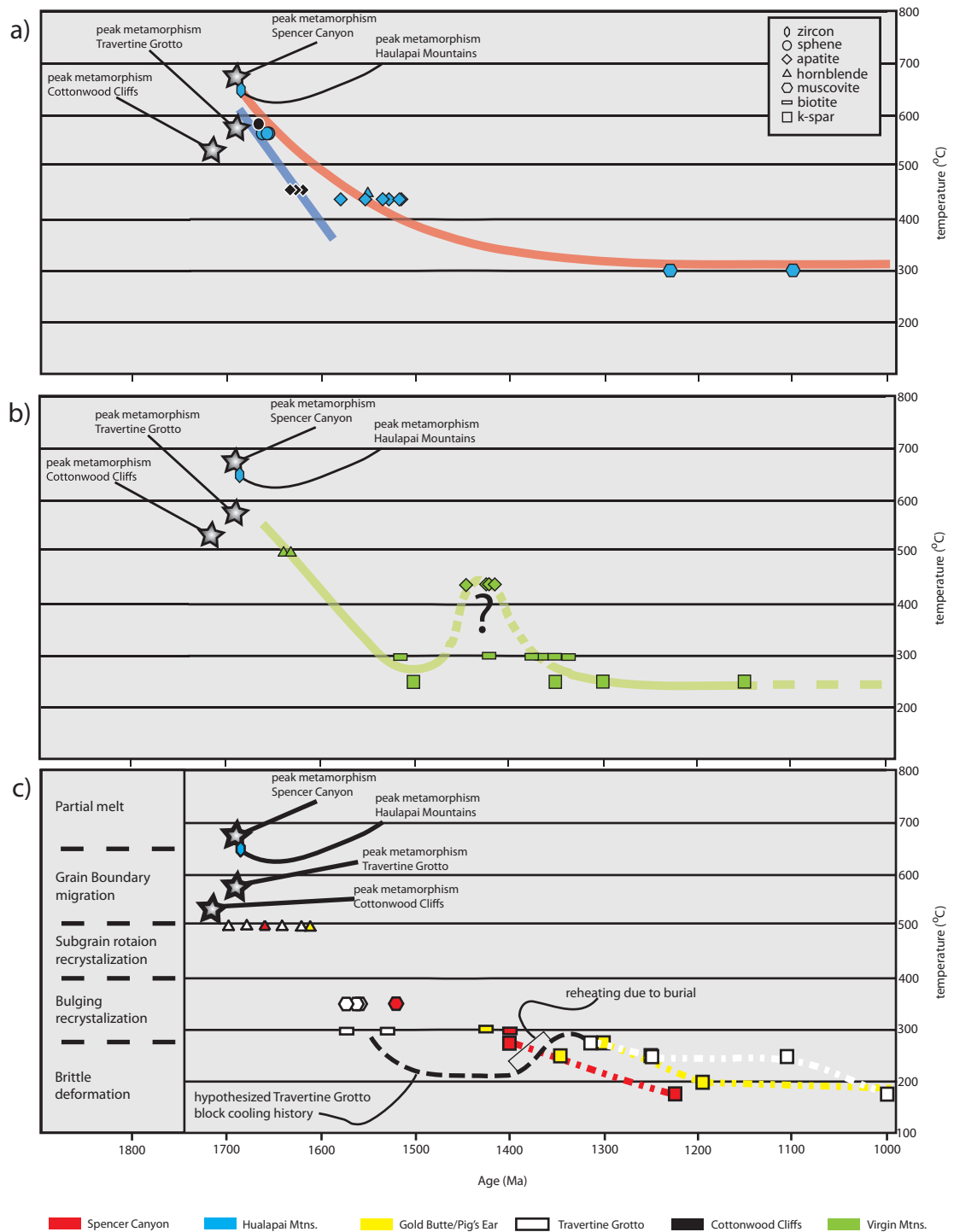


Figure 15. Time-temperature plot for crustal blocks within study area. R1, R2, and R3 refer to regime 1, 2, and 3 of Hirth and Tullis 1992. Age errors are smaller than symbols. Actual cooling temperature may vary from those plotted by ± 50 °C. Data from Chamberlain and Bowring 2001 (a), Quigley 2002 (b), this study and Karlstrom et. al. 2010 (c). See text for further discussion.

southeastern Nevada including the Hualapai Mountain, Cottonwood Cliffs, Gold Butte, and Virgin Mountain blocks. These data are summarized in Figure 15. The combined data from the Lower Gorge, Hualapai Mountain, Cottonwood Cliffs, Gold Butte, and Virgin Mountain blocks suggest that basement rocks near the Great Unconformity cooled through 500 °C by around 1600 Ma, following the Yavapai orogeny. In the Gold Butte and Virgin Mountain Block, K-spar total gas ages range from about 900-1400 Ma (Quigley, 2002). An MDD model from sample KGB 99-1 just below the Great Unconformity near the mouth of Grand Canyon in the Gold Butte block has an age gradient from 1300 to 650 Ma. A modeled cooling history that matches the measured spectrum has an initial periods of cooling from >300 to 200 °C between 1300 and 1150 Ma, an isothermal (180 °C) period from 1150 to 750 Ma, then cooling from 180 to near the surface between 1150 and 750 Ma prior to Tapeats Sandstone deposition about 540 Ma (Karlstrom et. al. 2010) (figure 15).

Biotites from the Virgin Mountain area gives plateau ages ranging from 1511 to 1336 Ma (Quigley, 2002) and 2 samples from the Gold Butte area giving ages of 1424 ± 2 Ma (Karlstrom et al., 2010) and 1374 ± 13 Ma (Reiners 2000). The combined biotite ages (n= 9) have a mean age of 1400 Ma. This is in marked contrast with the Travertine Grotto block where the mean of biotite ages is ca. 1550 Ma. This is interpreted to mean that the western blocks experienced slower cooling between 500 °C and 350 °C than the eastern block, and/or that the western block was reheated and reset at 1.4 Ga while the eastern block was not.

Data from the Gold Butte and north Virgin Mountain areas are more similar to the Spencer Canyon block. Hornblendes from the northern Virgin Mountains (Quigley, 2002)

give disturbed spectra with assigned plateau ages ranging from 1638-1524 (mean of five samples = 1620 Ma), perhaps slightly younger than the Travertine Grotto Block (1656 Ma) and Spencer Canyon block (1642 Ma). Muscovites from the Gold Butte block near the unconformity are 1385-1374 Ma with a mean of 1380 Ma (Reiners 2000, Karlstrom et. al. 2010).

In Grand Canyon, comparison of cooling histories from the Travertine Grotto and Spencer Canyon block suggest that western blocks cooled more slowly from hornblende (~500 °C) through muscovite (~350 °C) Ar closure temperatures than eastern blocks. This data is compatible with the different cooling curves published by Chamberlain and Bowring (1990, 2001; figure 15 a) based on apatite data, which suggested that the Cottonwood Cliffs (cold block; see figure 2) cooled through ca. 450 °C at 1630 Ma whereas the Hualapai Mountains (hot block, see figure 2) cooled through 450 °C between 1560 and 1510 Ma. Chamberlain and Bowring proposed that a crustal boundary lay between these blocks, and suggested that an isostatic mechanism, as outlined in Bowring and Karlstrom (1990), for juxtaposition of blocks with different thermal histories. In Grand Canyon, Gneiss Canyon shear zone separates such blocks. Biotites from the Travertine Grotto block have a mean age which is significantly older than the ages of the analyzed biotite from the Spencer Canyon, Gold Butte, and Virgin Mountain blocks and from Gneiss Canyon shear zone. This suggests that the difference in cooling paths of hot versus cold blocks persisted at least until about 1400 Ma.

Argon data from the Travertine Grotto block and Gneiss Canyon shear zone show muscovite ages ranging from 1573-1562 Ma and biotite ages from 1573-1531 Ma. Monazite ages associated with greenschist metamorphic assemblages from this time

period have been recorded in the Virgin Mountains (Quigley 2002), so it is possible that regime 1 and 2 quartz deformation may have occurred over this time interval. However, metamorphic and plutonic dates of this age are generally sparse in the region, and have not been found in western Grand Canyon. The lack of monazite dates in the range 1573 to 1531 Ma suggest that mica ages reflect migration through 350 °C and 300 °C isotherms rather than a partial resetting of closure dates by a later thermal event.

Several models have been published to explain the difference in cooling history between “hot” and “cold” blocks within the slowly cooled (Hodges et. al. 1994, Hodges and Bowring 1995) Proterozoic rocks of NW Arizona. These include: Variable isostatic responses following crustal assembly (Bowring and Karlstrom 1990), caused by differential heat production within adjacent blocks (Flowers et al., 2004, 2005). Long term mid-crustal residence (Heizler et. al. 2004) ± proximity to 1.4 Ga plutons (Nyman et. al. 1994, Shaw et. al. 2005) and 1.4 Ga shear zones that juxtapose different crustal levels (Dumond et al. 2003, this paper).

Syn and post-1.4 Ga cooling histories are a key dataset to evaluate these different models. Multiple diffusion domain (MDD) modeling of K-feldspar from western blocks show that Spencer Canyon cooled through temperatures of 275-175 °C from ca. 1400 to ca. 1200 Ma. The Gold Butte Block cooled to about 200 °C shortly after 1200 Ma followed by very slow apparent cooling from 200 °C to 175 °C by ~750 Ma (Karlstrom et. al. 2010). An MDD model from the Travertine Grotto block show cooling from 275 °C to ca. 250 °C between ca. 1300 Ma and ca. 1250 Ma followed by protracted residence at 250 °C until unroofing at coincident with ~1100 Ma tectonism. This reveals an apparent cross in cooling paths with an intersection occurring after 1.4 Ga. The dashed

black hypothesized curve for Travertine Grotto depicted in figure 15 c reflects a segment of the cooling curve that may be obscured by subsequent reheating due to burial associated with west-side-up thrusting of the Spencer Canyon block across the Gneiss Canyon shear zone at this time.

Possible thermal effects of 1.4 Ga tectonism

Initial rates of cooling after peak metamorphism in the northwestern Arizona and southeastern Nevada are relatively rapid, which suggests cooling following regional high heat flow and metamorphism. Between 500 and 300 °C cooling rates are reduced and curves for hot and cold blocks appear to diverge between muscovite cooling dates and biotite cooling dates (figure 15 c). This divergence between Spencer Canyon and Travertine Grotto biotite ages suggest either a change in crustal levels and/or some thermal perturbation, such as local reheating of the Spencer Canyon block similar to that hypothesized in Quigley (2002) for the Virgin Mountain block see 15 b.

One common attribute of 3 of the “hot” blocks (Hualapai Mountain, Gold Butte and Spencer Canyon) in the larger study region is that ~1.4 Ga granitic plutons outcrop in or near each of them. For example, in Spencer Canyon, K-feldspar ages are similar to the crystallization age of the 1375 Ma (Karlstrom et. al. 2003) Quartermaster granite. K-feldspar ages show cooling from ~275 °C between ca. 1425 Ma and 1375 Ma in Spencer, which allows the possibility of reheating at Spencer Canyon during emplacement of the Quartermaster, followed by a return to ambient conditions and continued slow cooling.

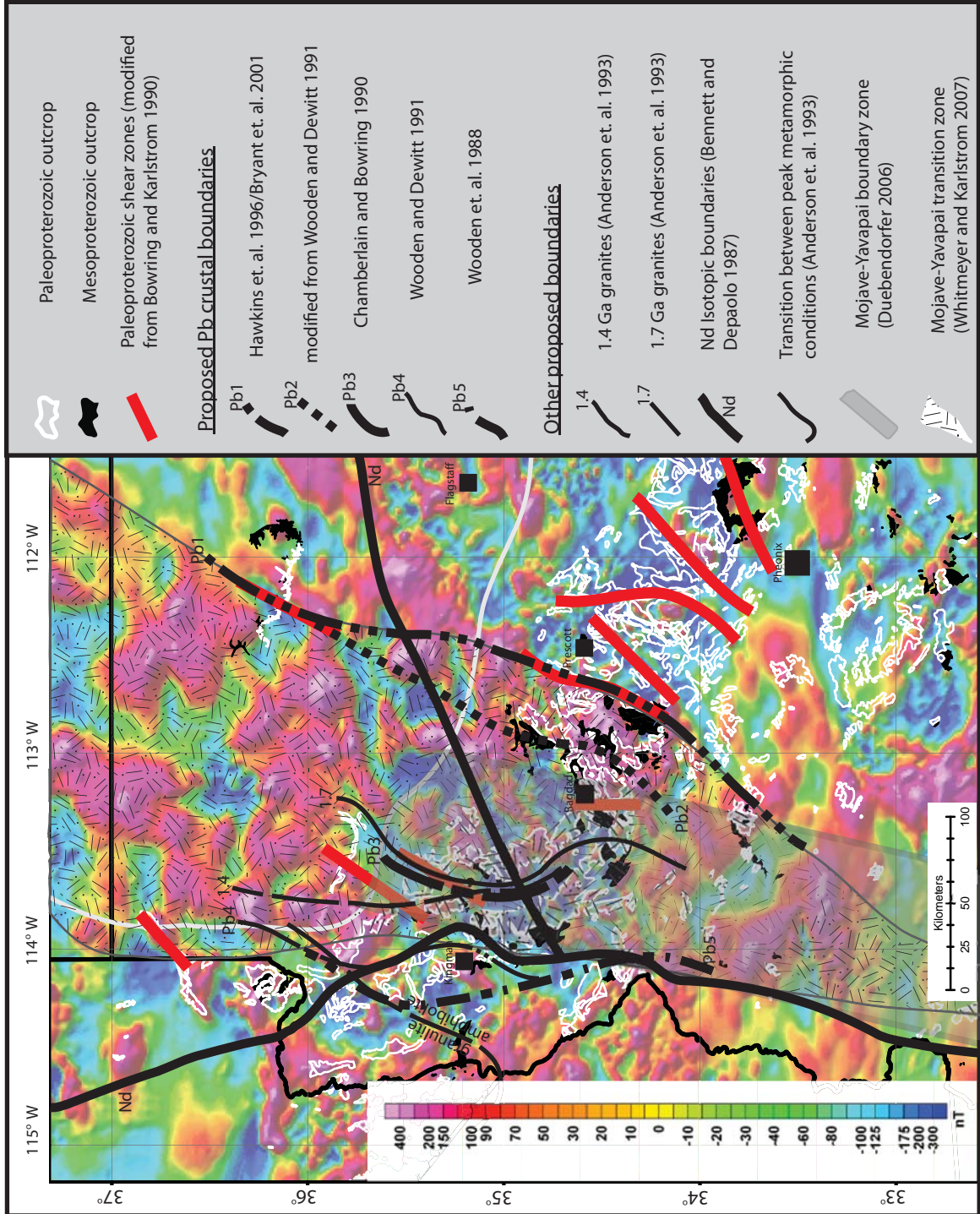
Plutons may cool to ambient temperatures ~1 Ma after emplacement (Paterson and Tobisch 1992), although sheet-like intrusion models (Glazner et al. 2004) suggest

pluton enhance heat can persist incrementally over tens of millions of years (Coleman et. al. 2004). Both the Quartermaster and Gold Butte granites have micas and/or K-feldspar ages near the unconformity very close to the crystallization age of nearby ~1.4 Ga granites, which are thought to have intruded at ~ 10 km. Therefore the geothermal gradient was likely between ~30-35 °C/km in the Spencer Canyon and Gold Butte areas during the time of emplacement

The nearest outcrop of the Quartermaster granite is over 6 km from Spencer Canyon sample location. At this distance, it would be difficult for heat from the Quartermaster pluton to effect argon cooling ages. However, estimates based on models of Jaeger (1959) and Parmentier and Schedl (1981) suggest that if the Quartermaster is modeled as a sheet with a width of ~5-9 km that intruded into country rock with ambient temperatures of ~300 °C/km, biotite and K-feldspar could be reset if Quartermaster granite sub-crops within 1-3 km of sample locations. A comparison of Quartermaster outcrop locality and regional aeromagnetic data (figure 16) suggest that this is plausible, but a more detailed geophysical investigation would be necessary to test this further. A similar comparison of the Gneiss Canyon shear zone and Travertine Grotto sampling localities at RM's 237 and 229 respectively suggests that a similar resetting by 1.4 Ga plutonism is less plausible, as closest observed 1.4 Ga plutonism is > 15 km for the Gneiss Canyon shear zone sample and > 26 kilometers away for Travertine Grotto.

Cooling data compiled by Shaw et. al. (2005) suggests that elevated geotherms existed throughout much of the southwestern U.S. at this time even in localities with a relative paucity of 1.45 Ga to 1.35 Ga plutons. This and the relatively small contact aureoles observed around plutons of this age suggest that the heating at this time was due

Figure 16. Aeromagnetic map of northwestern Arizona with proposed province boundary lines and zones. (Aeromagnetic data from Bankey et. al. 2002) See text for discussion



to a more regional thermal event that likely had a causal relationship with these plutons. So the lack of ~1.4 Ga resetting in the Travertine Grotto block may also suggest a shallower depth during this event. Shaw et al (2005) invokes a mid crustal melt fluid zone that may have separated hot, convectively flowing middle crust from a conductively cooling upper crust. Under this model, modest displacements on syn 1.4 shear zones could juxtapose rocks with slow cooled 1.6-1.4 Ga cooling history with rocks that experienced 1.4 Ga thermal resetting, as suggested by the alternate (reheating) cooling history shown in figure 15 b and c.

To explain the regional occurrence of blocks with different cooling histories as shown in Figure 15, a model involving a combination of 1.4-1.3 Ga displacement of blocks with markedly different pre-1.4 cooling histories across the Gneiss Canyon shear zone, and thermal pulses related to nearby 1.4 Ga plutonism is favored. Explanations for the different 1.6-1.4 Ga cooling histories involve some combination of 1) differential heat production, 2) pluton-added heat, and 3) steep thermal gradients associated with a mid crustal melt-fluid layer. MDD modeling data for Travertine Grotto blocks appears to show that #1 is less important in this locality after 1.4 Ga, as differential heat production would result in cooling paths that remain continue to diverge with western blocks cooling slower after 1.4 Ga. It appears that 2 and 3 may be a bit more plausible, as #2 predicts thermal histories with spikes related to 1.4 plutons, and #3 predicts thermal histories may converge after displacement at, or after, 1.4 Ga as shown in figure 15.

Links between microstructures, geochronology, and Ar cooling paths

Formation of observed D₂ west-side-up shear and associated high temperature microstructures in western Grand Canyon is interpreted to have initiated during or before, and continued after peak metamorphic conditions were attained during Yavapai tectonism (Robinson 1994, Hutchison 1996, Karlstrom et. al. 2003). Because deformation temperature estimates for feldspar ductility are > 500, it is inferred that these high temperature shear fabrics pre-dated 1.6 Ga. Monazite ages from the Gneiss Canyon shear zone of 1.7-1.63 Ga also suggest that higher T deformation was taking place over a long-lived progressive deformation.

A persistent question is whether cooling (with or without progressive ductile deformation) could have been taking place semi-continuously from 1.7-1.5 Ga to explain the 1.5 Ga 350 °C temperatures inferred from the Ar muscovite data, for example as inferred by Duebendorfer et. al. (2006b). Quigley (2002) reported 1.67-1.55 monazite microprobe ages associated with greenschist metamorphic assemblages in the Virgin Mountains, so regime 1 and 2 quartz deformation in Grand Canyon may have occurred over this time interval. However, metamorphic and plutonic dates of this age are generally sparse in the region, and have not been found in western Grand Canyon. The lack of monazite dates in the range ~1566 to ~1488 Ma suggest that mica ages reflect cooling through 350 °C and 300 °C isotherms due to unroofing or a regional reduction in geothermal gradients rather than continued deformation in Grand Canyon. Quigley (2002) also reported U-Pb apatite dates of 1446-1410 Ma from the Virgin Mountains. When combined with other data, this suggest a cooling path for the Virgins that involved reheating at 1425 Ma that might have been accompanied by partial resetting of monazite.

This model is depicted for the western blocks with a reheating spike rather than continuous cooling.

Quartz microstructures in Grand Canyon suggest temperatures of 300-400 °C and these overlap significantly with muscovite and biotite closure temperature (see 15 c) such that cooling dates from these minerals provide a first order estimation of minimum ages of ductile deformation. Our data suggest that final juxtaposition and formation of the lowest T ductile quartz fabrics occurred at temperatures near or below ~300 °C during D₃ deformation after ~1.4 Ga. The combined data seem best explained by a model for post-1.4 Ga reactivation of the Gneiss Canyon shear zone.

CONCLUSIONS

1) Microprobe monazite ages from Gneiss Canyon shear zone suggest that high temperature ductile deformation took place from about 1.7 to as late as 1.63 Ga during an up to 70-Ma-long set of deformation episodes that are interpreted to suggest that middle crustal deformation spanned both the 1.7- 1.68 Ga Yavapai and 1.65 Ga Mazatzal orogenies.

2) Discrete cm to m-scale mylonite zones, which occur within the higher temperature Gneiss Canyon shear zone, are interpreted to be retrograde reactivations of the shear zone.

- 3) Microstructures indicate west-side-up and dextral sense of shear on the lower-T mylonite zone, with an increased component of dextral strike slip-motion compared to the higher temperature shearing.

- 4) Temperature ranges estimated from feldspar ($> 500\text{ }^{\circ}\text{C}$) and quartz ($\sim 450 - < 300\text{ }^{\circ}\text{C}$) microstructures overlap with argon cooling ages for hornblende ($500\text{ }^{\circ}\text{C}$), muscovite ($350\text{ }^{\circ}\text{C}$), biotite ($300\text{ }^{\circ}\text{C}$), and K-feldspar ($275\text{-}175\text{ }^{\circ}\text{C}$). These data suggest that highest T microstructures developed before $\sim 1600\text{ Ma}$, whereas low T microstructures developed after 1500 in the eastern block and after 1400 in the western blocks.

- 5) The possibility of a single progressive deformation from 1700-1400 Ma is not favored here because of overprinting of low T quartz microstructures on high temperature feldspar microstructures, and because the different thermal histories of blocks east and west of the Gneiss Canyon shear zone from 1650-1400, and the similar cooling histories after 1350 Ma.

- 6) The preferred explanation for the combined evidence is a final juxtaposition of blocks to the same elevation, and hence similar cooling histories after 1.4 Ga. Pluton enhanced resetting of micas and K-feldspars at 1.45-1.35 Ga (e.g. the 1375 Ma Quartermaster pluton) is not required in this model, but may help explain pervasive 1.4 Ga biotite ages in the western blocks. K-feldspar MDD cooling curves from blocks east and west of the Gneiss Canyon shear zone suggest burial of the Travertine Grotto block as a result of west-side-up shearing, followed by unroofing related to 1.1 Ga tectonism.

REFERENCES CITED

- Albin, A. L., 1991, Structural Geology of the Gneiss Canyon shear zone in the Peacock Mountains and Southern Grand Wash Cliffs, northwestern Arizona, [M.S. thesis], Flagstaff, Northern Arizona University, 68 p.
- Albin, A.A., and Karlstrom, K.E., 1991, Orthogonal Proterozoic fabrics in northwestern Arizona: Multiple orogenic events or progressive deformation during continental assembly, in Karlstrom, K.E. ed., Proterozoic geology and ore deposits of Arizona: Arizona Geological Society Digest 19, p. 67-84.
- Anderson, J.L., Wooden, J.L., and Bender, E.E., 1993, Mojave province of southern California and vicinity, in Van Schmus, W.R., and 24 others, 1993: Transcontinental Proterozoic provinces, in Reed, J.C., Jr., Bickford, M.E., Houston, R.S., Link, P.K., Rankin, D.W., Sims, P.K., and Van Schmus, W.R., eds., Precambrian: Conterminous U.S.: Boulder, Colorado, Geological Society of America, The Geology of North America C-2, p. 176-188.
- Bankey, V., Cuevas, A., Daniels, D., Finn, C. A., Hernandez, I., Hill, P., Kucks, R., Miles, W., Pilkington, M., Roberts, C., Roest, W., Rystrom, V., Shearer, S., Snyder, S., Sweeney, R., Velez J., Phillips, J.D. and Ravat, D., 2002, Digital data grids for the magnetic anomaly map of North America: U.S. Geological Survey Open-File Report 02-414 (DVD).
- Bennett, V.C., and DePaolo, D.J., 1987, Proterozoic crustal history of the western United States as determined by neodymium isotopic mapping: Geological Society of America Bulletin, v. 99, p. 674-685.
- Bickford, M. E., and Hill, B. M., 2007, Does the arc accretion model adequately explain the Paleoproterozoic evolution of southern Laurentia?: An expanded interpretation: Geology, v. 35, no. 2, p. 167-170.
- Bowring, S. A., and Karlstrom, K. E., 1990, Growth, stabilization, and reactivation of Proterozoic lithosphere in the southwestern United-States: Geology, v. 18, no. 12, p. 1203-1206.
- Bryant, B., Wooden, J. L., & Nealey, L. D., 2001. Geology, geochronology, geochemistry, and Pb-isotopic compositions of Proterozoic rocks, Poachie region, west-central Arizona; A study of the east boundary of Proterozoic Mojave crustal province. U.S. Geological Survey Professional Paper 1639, 62 p.
- Chamberlain, K. R., and Bowring, S. A., 1990, Proterozoic geochronological and isotopic boundary in NW Arizona: Journal of Geology, v. 98, no. 3, p. 399-416.

- Chamberlain, K. R., and Bowring, S. A., 2001, Apatite-feldspar U-Pb thermochronometer: a reliable, mid-range (similar to 450 degrees C), diffusion-controlled system: *Chemical Geology*, v. 172, no. 1-2, p. 173-200.
- Coleman, D.S., Gray, W., Glazner, A. F., 2004, Rethinking the emplacement and evolution of zoned plutons: Geochronologic evidence for incremental assembly of the Tuolumne Intrusive Suite, California: *Geology*, v. 32, p. 433-436
- Collins, W., Vernon, R., Clarke, G., 1991, Discrete Proterozoic structural terranes associated with low-p, high-t metamorphism, Anmatjira range, Arunta Inlier, central Australia - tectonic implications: *Journal of Structural Geology*, v. 13, p. 1157-1171
- Duebendorfer, E. M., Chamberlain, K. R., and Fry, B., 2006a, Mojave-Yavapai boundary zone, southwestern United States: A rifting model for the formation of an isotopically mixed crustal boundary zone: *Geology*, v. 34, no. 8, p. 681-684.
- Duebendorfer, E. M., Chamberlain, K. R., and Heizler, M. T., 2006b, Filling the North American Proterozoic tectonic gap: 1.60-1.59-Ga deformation and orogenesis in southern Wyoming, USA: *Journal of Geology*, v. 114, no. 1, p. 19-42.
- Dumond, G., Williams, M., Karlstrom, K. E., Heizler, M., Mahan, K., 2003, Constraining the tectonic history of the Proterozoic Mojave-Yavapai province boundary; insights from detailed metamorphic petrology and monazite geochronology along a transect across the 96-mile and Crystal shear zones of the Upper Granite Gorge, Grand Canyon, Arizona. Abstracts with Programs - Geological Society of America, 35(5), 42-42.
- Dumond, G., Mahan, K. H., Williams, M. L., and Karlstrom, K. E., 2007, Crustal segmentation, composite looping pressure-temperature paths, and magma-enhanced metamorphic field gradients: Upper Granite Gorge, Grand Canyon, USA: *Geological Society of America Bulletin*, v. 119, no. 1-2, p. 202-220.
- Dunlap, W. J., Hirth, G., and Teyssier, C., 1997, Thermomechanical evolution of a ductile duplex: *Tectonics*, v. 16, no. 6, p. 983-1000.
- Ferguson, C. B., Duebendorfer, E. M., and Chamberlain, K. R., 2004, Synkinematic intrusion of the 1.4-Ga Boriana Canyon pluton, northwestern Arizona: Implications for ca. 1.4-Ga regional strain in the western United States: *Journal of Geology*, v. 112, no. 2, p. 165-183.
- Flowers, R. M., Royden, L. H., and Bowring, S. A., 2004, Isostatic constraints on the assembly, stabilization, and preservation of cratonic lithosphere: *Geology*, v. 32, no. 4, p. 321-324.

- Flowers, R.M., Royden, L.H., and Bowring, S.A., 2005, Isostatic constraints on lithospheric thermal evolution: Application to the Proterozoic orogen of the southwestern United States, in Karlstrom, K.E. and Keller, R.G., eds., The Rocky Mountain region: An evolving lithosphere: Tectonics, geochemistry and geophysics: American Geophysical Union Monograph 154, p. 125-138.
- Glazner, A F; Bartley, J M; Coleman, D S; Gray, W; Taylor, R Z., 2004 Are plutons assembled over millions of years by amalgamation from small magma chambers?: GSA Today, v. 14, p. 4-11
- Hawkins, D.P., Bowring, S.A., Ilg, B.R., Karlstrom, K.E., and Williams, M.L., 1996, U-Pb geochronologic constraints on the Paleoproterozoic crustal evolution of the Upper Granite Gorge, Grand Canyon, Arizona: Geological Society of America Bulletin, v. 108, p. 1167- 1181.
- Heizler M. T., Karlstrom K. E., Shaw C. A., Timmons J. M., and Sanders R. E., 2004, The evolution of Laurentia as documented by $^{40}\text{Ar}/^{39}\text{Ar}$ thermochronology studies Abstracts with Programs - Geological Society of America, 36(5), 405.
- Hirth, G., and Tullis, J., 1992, Dislocation creep regimes in quartz aggregates: Journal of Structural Geology, v. 14, no. 2, p. 145-159.
- Hobbs, B. E., Means, W. D., and Williams, P.F., 1976, An outline of structural geology. New York, Wiley, 512 p.
- Hodges, K. V., Hames, W. E., and Bowring, S. A., 1994, $^{40}\text{Ar}/^{39}\text{Ar}$ age gradients in micas from a high-temperature low-pressure metamorphic terrain - evidence for very slow cooling and implications for the interpretation of age spectra: Geology, v. 22, no. 1, p. 55-58.
- Hodges, K. V., and Bowring, S. A., 1995, $^{40}\text{Ar}/^{39}\text{Ar}$ thermochronology of isotopically zoned micas - insights from the southwestern USA Proterozoic orogen: Geochimica Et Cosmochimica Acta, v. 59, no. 15, p. 3205-3220.
- Hutchison, J. L., 1996, Relative timing of porphyroblast growth and peak metamorphism in the Lower granite Gorge, Grand Canyon, Arizona: (M.S. thesis), Albuquerque, University of New Mexico, 59 p
- Ilg, Brad, Karlstrom, K.E., Hawkins, D., and Williams, M.L., 1996, Tectonic evolution of Paleoproterozoic rocks in Grand Canyon, Insights into middle crustal processes: Geological Society of America Bulletin, v. 108, p. 1149-1166.
- Iriondo, A., Premo, W. R., Martinez-Torres, L. M., Budahn, J. R., Atkinson, W. W., Siems, D. F., and Guaras-Gonzalez, B., 2004, Isotopic, geochemical, and temporal characterization of Proterozoic basement rocks in the Quitovac region,

- northwestern Sonora, Mexico: Implications for the reconstruction of the southwestern margin of Laurentia: *Geological Society of America Bulletin*, v. 116, no. 1-2, p. 154-170.
- Jaeger, J. C., 1959, Temperatures outside - a cooling intrusive sheet: *American Journal of Science*, v. 257, no. 1, p. 44-54.
- Karlstrom, K. E., Bowring, S. A., and Conway, C. M., 1987, Tectonic significance of an early Proterozoic 2-province boundary in central Arizona: *Geological Society of America Bulletin*, v. 99, no. 4, p. 529-538.
- Karlstrom, K. E., and Bowring, S. A., 1988, Early Proterozoic assembly of tectonostratigraphic terranes in southwestern North-America: *Journal of Geology*, v. 96, no. 5, p. 561-576.
- Karlstrom, K.E., and Bowring, S. A., 1991, Styles and timing of early Proterozoic deformation in Arizona: Constraints on tectonic models, in Karlstrom, K.E., ed., *Proterozoic geology and ore deposits of Arizona: Arizona Society Digest*, v. 19, p. 1-10.
- Karlstrom, K.E., and Bowring, S. A., 1993, Proterozoic orogenic history in Arizona, in Van Schmus, W.R., et al., *Transcontinental Proterozoic provinces*, in Reed, J.C., Jr., Bickford, M.E., Houston, R.S., Link, P.K., Rankin, D.W., Sims, P.K., and Van Schmus, W.R., eds., *Precambrian: Conterminous U.S.: Boulder, Colorado, Geological Society of America, The Geology of North America*, v. C-2. p. 188-211
- Karlstrom, K.E., and Humphreys, G., 1998, Influence of Proterozoic accretionary boundaries in the tectonic evolution of western North America: Interaction of cratonic grain and mantle modification events: *Rocky Mountain Geology*, v. 33, no.2, p. 161-179.
- Karlstrom, K.E., Ilg, B.R., Williams, M.L., Hawkins, D.P., Bowring, S.A., Seaman, S.J., 2003, Paleoproterozoic rocks of the Granite Gorges, in Beus, S.S. and Morales, M., eds., *Grand Canyon Geology (2nd edition)*: Oxford, Oxford University Press, p. 9-38.
- Karlstrom, K. E., and Williams, M. L., 1995, The case for simultaneous deformation, metamorphism and plutonism - an example from Proterozoic rocks in central Arizona: *Journal of Structural Geology*, v. 17, no. 1, p. 59-81.
- Karlstrom, K.E. and Williams, M.L., 2006, Nature of the middle crust—heterogeneity of structure and process due to pluton-enhanced tectonism: an example from Proterozoic rocks of the North American Southwest, in Brown, M. and Rushmere, T., eds., *Evolution and differentiation of the continental crust*: Cambridge University Press, p. 268-295.

- Karlstrom, K.E., Heizler, M., and Quigley, M.C., 2010, Structure and $^{40}\text{Ar}/^{39}\text{Ar}$ K-feldspar thermal history of the Gold Butte block: Reevaluation of the tilted crustal section model, in Umhoefer, P.J., Beard, L.S., and Lamb, M.A., eds., Miocene Tectonics of the Lake Mead Region, Central Basin and Range: Geological Society of America Special Paper 463, p. 331–352
- Lee, C., Yin, Q., Rudnick, R. L., & Jacobsen, S. B., 2001. Preservation of ancient and fertile lithospheric mantle beneath the southwestern United States. *Nature*, 411(6833), 69-73.
- Lister, G. S., and Snoke, A. W., 1984, S-C mylonites: *Journal of Structural Geology*, v. 6, no. 6, p. 617-638.
- McDougall, I., and Harrison, T.M., 1999, Geochronology and Thermochronology by the $^{40}\text{Ar}/^{39}\text{Ar}$ Method: New York, Oxford University Press, 269 p.
- Nyman, M. W., Karlstrom, K. E., Kirby, E., and Graubard, C. M., 1994, Mesoproterozoic contractional orogeny in western North-America - evidence from ca-1.4-Ga plutons: *Geology*, v. 22, no. 10, p. 901-904.
- Parmentier, E. M., and Schedl, A., 1981, Thermal aureoles of igneous intrusions - some possible indications of hydrothermal convective cooling: *Journal of Geology*, v. 89, no. 1, p. 1-22.
- Passchier, C.W., and Trouw, R.A.J., 1996, *Microtectonics*: Berlin, Springer-Verlag, 289 p.
- Paterson, S. R., and Tobisch, O. T., 1992, Rates of processes in magmatic arcs - implications for the timing and nature of pluton emplacement and wall rock deformation: *Journal of Structural Geology*, v. 14, no. 3, p. 291-300.
- Quigley, M.C., 2002, Tectonic Development of Proterozoic Structures and their Influence on Laramide and Miocene Deformation, North Virgin Mountains, SE Nevada and NW Arizona [M.S. thesis]: Albuquerque, University of New Mexico, 194 p.
- Ramo, O. T., and Calzia, J. P., 1998, Nd isotopic composition of cratonic rocks in the southern Death Valley region: Evidence for a substantial Archean source component in Mojavia: *Geology*, v. 26, no. 10, p. 891-894.
- Reiners, P. W., Brady, R., Farley, K. A., Fryxell, J. E., Wernicke, B., and Lux, D., 2000, Helium and argon thermochronometry of the Gold Butte block, south Virgin Mountains, Nevada: *Earth and Planetary Science Letters*, v. 178, no. 3-4, p. 315-326.

- Reynolds, S.J., 1988, Geologic Map of Arizona: Arizona Geological Survey Map 26, scale 1:1,000,000
- Robinson, K., 1994, Metamorphic petrology of the Lower Granite Gorge and the significance of the Gneiss Canyon shear zone, Grand Canyon: Amherst, University of Massachusetts, [master's thesis], 187 p
- Sanders, R.E. and Heizler, M.T., Goodwin, L.B., 2006, $^{40}\text{Ar}/^{39}\text{Ar}$ thermochronology constraints on the timing of Proterozoic basement exhumation and fault ancestry, southern Sangre de Cristo Range, New Mexico: GSA Bulletin; v. 118 p. 1489–1506
- Shaw, C.A., Heizler, M.H., Karlstrom, K.E., 2005. $^{40}\text{Ar}/^{39}\text{Ar}$ Thermochronologic Record of 1.45-1.35 Ga Intracontinental Tectonism in the Southern Rocky Mountains: Interplay of Conductive and Advective Heating With Intracontinental Deformation, in Karlstrom, K.E. and Keller, G.R., eds., The Rocky Mountain Region -- An Evolving Lithosphere: Tectonics, Geochemistry, and Geophysics, American Geophysical Union Monograph 154, p. 163-184.
- Shufeldt, O.P., Karlstrom, K.E., Gehrels, G.E., (in press) Predominance of 1.84 Ga and >2.5 Ga detrital zircons in the 1.75 Ga Vishnu schist, Upper Granite Gorge, Grand Canyon, Arizona. *Geology*
- Simpson, C., and Depaor, D. G., 1993, Strain and kinematic analysis in general shear zones: *Journal of Structural Geology*, v. 15, no. 1, p. 1-20
- Stevens, L. 1983, The Colorado River in Grand Canyon, Red Lake Books, Flagstaff, AZ, 115p.
- Stipp, M., Stunitz, H., Heilbronner, R., and Schmid, S.M., 2002, The eastern Tonale fault zone: a 'natural laboratory' for crystal plastic deformation of quartz over a temperature range from 250 to 700 degrees C: *Journal of Structural Geology*, v. 24, p. 1861-1884.
- Stockhert, B., Brix, M. R., Kleinschrodt, R., Hurford, A. J., and Wirth, R., 1999, Thermochronometry and microstructures of quartz - a comparison with experimental flow laws and predictions on the temperature of the brittle-plastic transition: *Journal of Structural Geology*, v. 21, no. 3, p. 351-369.
- Timmons, J. M., Karlstrom, K. E., Heizler, M. T., Bowring, S. A., Gehrels, G. E., and Crossey, L. J., 2005, Tectonic inferences from the ca. 1255-1100 Ma Unkar Group and Nankoweap Formation, Grand Canyon: Intracratonic deformation and basin formation during protracted Grenville orogenesis: *Geological Society of America Bulletin*, v. 117, no. 11-12, p. 1573-1595.

- Tullis, J., 2002, Deformation of Granitic Rocks: Experimental Studies and Natural Examples Reviews in Mineralogy and Geochemistry; v. 51; 1; p. 51-95
- Tullis, J., and Yund, R. A., 1985, Dynamic recrystallization of feldspar - a mechanism for ductile shear zone formation: *Geology*, v. 13, no. 4, p. 238-241.
- Tullis, J., Stunitz, H., Teyssier, C., & Heilbronner, R., 2000: Deformation structures in Quartzofeldspathic rocks. In Jessel M.W. & Urai, J.L. (eds.): *Stress, Strain, and Structure. A volume in Honour of W.D. Means. Journal of the Virtual Explorer*, 2 (print and CD)
- Twichell, David C. , and Cross, VeeAnn A., 2003, Shapefile for the shoreline of Lake Mead: Interstate layers,
<http://pubs.usgs.gov/of/2009/1150/gis/basemap/lakebnds.zip>
- U.S. Geologic Survey, 2005, Preliminary integrated geologic map databases for the United States - western states: California, Nevada, Arizona, Washington, Oregon, Idaho, and Utah: U.S. Geologic Survey Open-File Report 2005-1305,
<http://pubs.usgs.gov/of/2005/1305/>
- Vernon, R.H., 2004, A practical guide to rock microstructure: New York, Cambridge University Press, 594 p.
- Vernon, R.H., Clarke, G.L., and Collins, W.J., 1990, Mid-crustal granulite facies metamorphism: Low-pressure metamorphism and melting, Mount Stafford, central Australia, in Ashworth, J.R., and Brown, M., eds., High-temperature metamorphism and crustal anatexis: Mineralogical Society of Great Britain and Ireland Special Publication 2, p. 272-319.
- Vignerresse, J. L., 1995, Far-field and near-field deformation and granite emplacement: *Geodynamica Acta*, v. 8, no. 4, p. 211-227
- Whitmeyer, S. J. and Karlstrom, K. E., 2007, Tectonic model for the Proterozoic growth of North America: *Geosphere*, v. 3, no. 4, p. 220-259.
- Williams, M.L., 1991, Overview of Early Proterozoic Metamorphism in Arizona. In Karlstrom, K.E. (ed.), *Proterozoic Geology and Ore Deposits of Arizona*, Arizona Geological Society Digest 19, p.11-26.
- Williams, M. L., Jercinovic, M. J., and Hetherington, C. J., 2007, Microprobe monazite geochronology: Understanding geologic processes by integrating composition and chronology: *Annual Review of Earth and Planetary Sciences*, v. 35, p. 137-175.
- Wooden, J. L.; Stacey, J.S.; Doe, B. R.; Howard, K. A.; and Miller, D. M., 1988. Pb isotopic evidence for the formation of Proterozoic crust in the southwestern United States, in ERNST, W. G., ed., *Metamorphic and crustal evolution of the western U.S.*, Rubey Volume VII, Prentice Hall, p, 68-86.

Wooden, J.L., and DeWitt, E., 1991, Pb isotope evidence for a major Early Proterozoic crustal boundary in western Arizona, In: Karlstrom, K.E., ed., Proterozoic geology and ore deposits of Arizona: Arizona Geological Society Digest, v. 19, p. 27-50.

Zulauf, G., 2001, Structural style, deformation mechanisms and paleodifferential stress along an exposed crustal section: constraints on the rheology of quartzofeldspathic rocks at supra- and infrastructural levels (Bohemian Massif): Tectonophysics, v. 332, no. 1-2, p. 211-237

APPENDIX -- ⁴⁰Ar/³⁹Ar DATA TABLES

ID	Temp/Power (°C)/W	⁴⁰ Ar/ ³⁹ Ar	³⁷ Ar/ ³⁹ Ar	³⁶ Ar/ ³⁹ Ar (x 10 ⁻³)	K/Ca	⁴⁰ Ar* (%)	³⁹ Ar (%)	Age (Ma)	±1σ (Ma)
H98-208-2 A:10:107 , Hornblende, 1.68 mg, J=0.0159896±0.10%, D=1.0024±0.001, NM-107, Lab#=50292-02									
X A	750	139.1	2.853	249.8	0.18	47.1	0.8	1310.5	26.2
X B	850	99.71	1.746	81.00	0.29	76.1	1.3	1452.3	34.3
X C	950	78.57	2.333	20.14	0.22	92.7	2.6	1411.0	12.6
X D	1000	77.29	5.280	3.473	0.097	99.2	4.2	1464.9	9.2
X E	1050	96.60	16.83	10.34	0.030	98.2	17.2	1698.6	2.8
F	1080	96.32	16.98	5.742	0.030	99.6	66.1	1711.4	2.1
X G	1100	89.32	15.33	6.553	0.033	99.2	69.4	1622.8	6.4
H	1120	93.53	16.76	1.623	0.030	100.9	70.6	1692.8	11.9
I	1140	94.52	17.33	5.796	0.029	99.7	72.4	1690.9	8.6
J	1160	97.67	17.62	3.453	0.029	100.4	73.7	1735.8	9.4
K	1200	97.73	18.09	5.701	0.028	99.8	76.6	1729.7	5.5
L	1250	96.46	17.01	4.523	0.030	100.0	80.5	1717.3	5.1
M	1650	96.59	17.31	7.027	0.029	99.3	100.0	1710.7	2.6
Integrated age ± 1σ		n=13			0.031			1695.8	2.2
Plateau ± 1σ		steps F-M	n=7				79.5	1712	2
T02-221-1musc J:1:158 , Muscovite, wt. = 0.55 mg, J=0.0114843±0.78%, D=1.00743±0.00124, NM-158, Lab#=53641-01									
X C	2	123.6	0.3872	102.4	1.3	75.5	0.2	1330.5	8.1
X D	2	118.6	0.5933	43.60	0.86	89.2	0.5	1452.4	5.8
X E	2	113.7	0.2433	23.26	2.1	94.0	0.7	1462.5	7.2
X F	3	110.4	0.1845	8.236	2.8	97.8	0.8	1472.7	10.6
G	3	114.4	0.0232	3.117	22.0	99.2	3.8	1523.6	2.8
H	4	117.3	0.0050	0.7175	101.3	99.8	5.4	1555.5	2.8
I	4	119.9	0.0034	0.6240	148.3	99.8	7.3	1578.9	4.6
J	4	120.1	0.0047	0.2195	109.1	99.9	10.0	1582.3	2.8
K	5	117.9	0.0021	0.3667	242.7	99.9	17.5	1562.1	2.4
L	6	114.9	0.0017	0.4687	297.7	99.9	25.4	1535.2	3.3
M	8	123.0	0.0014	0.4292	376.3	99.9	37.6	1606.7	3.7
N	10	120.2	0.0007	0.1972	763.7	100.0	51.1	1583.4	2.7
O	20	118.2	0.0009	3.791	594.2	99.1	96.7	1555.5	3.4
P	30	115.0	0.0049	3.189	104.2	99.2	100.0	1528.9	3.1
Integrated age ± 1σ		n=14			98.0			1562.9	8.5
Plateau ± 1σ		steps G-P	n=10				99.2	1564	2

ID	Temp/Power (°C)/W	⁴⁰ Ar/ ³⁹ Ar	³⁷ Ar/ ³⁹ Ar	³⁶ Ar/ ³⁹ Ar (x 10 ⁻³)	K/Ca	⁴⁰ Ar* (%)	³⁹ Ar (%)	Age (Ma)	±1σ (Ma)
H225-4 , I8, NM-128, hornblende, 2.02 mg, J=0.0165536±0.09%, D=1.006±0.0014, NM-128, Lab#=51576-01									
X A	3	79.04	0.6546	11.81	0.78	95.7	7.6	1482.3	2.8
B	5	86.58	7.511	3.193	0.068	99.6	44.5	1625.3	2.6
C	6	88.09	7.080	2.548	0.072	99.8	70.4	1645.6	3.1
X D	6	83.87	6.184	2.651	0.083	99.7	78.6	1590.8	2.6
X E	7	83.66	6.269	2.168	0.081	99.9	83.6	1590.0	2.8
X F	7	84.23	6.552	2.599	0.078	99.7	86.3	1596.2	3.3
X G	8	85.12	7.094	2.642	0.072	99.8	87.5	1608.2	6.0
M	16	89.17	9.452	3.340	0.054	99.8	100.0	1660.2	2.3
Integrated age ± 1σ			n=8		0.074			1618.9	2.2
Plateau ± 1σ			steps B-M	n=3			75.2	1638	3
H225-5A , K2, NM-128, hornblende, 1.6 mg, J=0.0165388±0.09%, D=1.006±0.0014, NM-128, Lab#=51580-01									
X A	3	148.2	3.050	21.48	0.17	95.9	6.0	2210.1	5.1
X B	5	98.36	9.883	6.890	0.052	98.7	17.3	1756.9	3.2
X C	6	105.8	10.80	5.599	0.047	99.3	25.0	1846.8	3.5
X D	6	106.8	12.90	4.892	0.040	99.6	33.4	1864.2	3.9
X E	7	102.1	12.45	4.734	0.041	99.6	39.9	1811.9	3.8
X F	7	108.8	12.35	5.559	0.041	99.4	45.1	1882.6	4.0
X G	8	103.8	12.78	4.711	0.040	99.6	49.4	1831.5	4.7
X H	9	105.8	12.24	6.114	0.042	99.2	54.4	1847.5	4.4
X I	9	123.9	14.21	4.820	0.036	99.8	58.0	2044.7	5.6
X J	10	108.2	15.27	4.646	0.033	99.9	61.3	1884.4	5.5
X K	10	98.93	14.00	6.971	0.036	99.1	63.5	1770.2	6.9
X L	13	102.6	11.76	4.203	0.043	99.7	75.3	1817.3	3.1
X M	16	130.6	12.92	6.814	0.039	99.3	78.6	2102.5	6.1
X N	30	125.9	14.26	8.363	0.036	98.9	100.0	2054.2	2.6
Integrated age ± 1σ			n=14		0.042			1919.5	2.4
Plateau ± 1σ			no plateau						

ID	Temp/Power (°C)/W	⁴⁰ Ar/ ³⁹ Ar	³⁷ Ar/ ³⁹ Ar	³⁶ Ar/ ³⁹ Ar (x 10 ⁻³)	K/Ca	⁴⁰ Ar* (%)	³⁹ Ar (%)	Age (Ma)	±1σ (Ma)
H225-5C I:4:128 , K-feldspar, 1.15 mg, J=0.01666±0.09%, D=1.006±0.0014, NM-128, Lab#=51573-01									
X A	525	411.2	0.0395	83.61	12.9	94.0	0.2	3664.5	13.0
X B	525	34.32	-0.0924	8.100	-	93.0	0.3	778.1	14.8
X C	525	27.33	-0.0883	14.39	-	84.4	0.4	593.4	15.2
X D	575	24.98	0.0544	2.313	9.4	97.3	0.7	620.3	6.7
X E	575	19.65	0.0553	3.862	9.2	94.2	0.9	490.4	5.8
X F	575	20.33	0.0527	7.960	9.7	88.4	1.2	477.9	6.5
X G	625	23.56	0.1012	2.507	5.0	96.9	1.6	588.0	4.0
X H	625	19.95	0.0804	2.996	6.3	95.6	1.9	503.2	4.8
X I	625	22.39	0.0874	1.565	5.8	98.0	2.2	568.2	4.8
X J	675	29.44	0.1154	2.575	4.4	97.4	3.0	713.0	2.5
X K	675	27.19	0.0716	1.351	7.1	98.6	3.8	673.5	2.4
X L	675	30.09	0.0144	2.656	35.5	97.4	4.3	725.6	3.5
X M	725	38.67	0.0275	2.207	18.6	98.3	5.5	895.7	2.0
X N	725	37.19	0.0346	1.028	14.8	99.2	6.4	874.4	2.3
X O	725	40.29	0.0458	1.549	11.1	98.9	7.0	929.1	3.2
X P	775	43.28	0.0549	1.074	9.3	99.3	8.1	985.5	2.3
X Q	775	45.51	0.0148	1.277	34.4	99.2	9.0	1023.6	2.9
X R	825	48.46	0.0038	1.572	135.7	99.0	10.3	1072.6	2.4
X S	825	49.87	-0.0009	1.196	-	99.3	11.5	1098.1	2.3
X T	875	50.92	0.0082	1.171	62.1	99.3	13.0	1115.7	2.1
X U	875	51.29	0.0046	0.9419	111.6	99.5	14.4	1122.9	2.2
X V	925	50.16	0.0195	1.480	26.2	99.1	17.1	1101.5	1.7
X W	925	50.69	0.0169	0.8434	30.2	99.5	19.5	1113.4	1.7
X X	975	49.79	0.0554	0.9772	9.2	99.4	22.3	1097.9	1.7
X Y	975	50.83	0.0210	0.9836	24.3	99.4	25.0	1115.1	1.9
X Z	1025	49.29	0.0221	0.9545	23.0	99.4	28.3	1089.7	1.7
X ZA	1025	50.41	0.0129	1.139	39.7	99.3	31.8	1107.4	1.7
X ZB	1075	48.86	0.0170	1.027	30.1	99.4	36.0	1082.1	1.7
X ZC	1075	51.48	0.0175	1.108	29.2	99.4	40.7	1125.3	1.7
X ZD	1125	51.10	0.0269	1.231	19.0	99.3	45.9	1118.5	1.6
X ZE	1125	54.24	0.0338	1.538	15.1	99.2	50.1	1168.0	1.7
X ZF	1175	54.50	0.0542	1.179	9.4	99.4	57.1	1173.9	1.7
X ZG	1175	57.39	0.0241	0.8184	21.2	99.6	67.6	1221.3	1.9
X ZH	1175	59.96	0.0164	0.8331	31.1	99.6	80.5	1260.7	1.6
X ZI	1175	61.76	0.0148	1.481	34.4	99.3	90.3	1285.1	1.9
X ZJ	1175	63.94	0.0228	6.162	22.3	97.2	94.5	1297.1	2.0
X ZK	1275	61.97	0.0123	0.7910	41.5	99.6	95.8	1291.2	2.3
X ZL	1325	62.98	0.0516	1.395	9.9	99.4	97.1	1303.9	2.5
X ZM	1375	62.26	0.0305	1.646	16.7	99.2	98.2	1291.9	2.6
X ZN	1775	63.21	0.0057	3.252	90.3	98.5	100.0	1299.0	2.4
Integrated age ± 1σ		n=40			20.1			1172.1	1.5
Plateau ± 1σ		no plateau							

ID	Temp/Power (°C)/W	⁴⁰ Ar/ ³⁹ Ar	³⁷ Ar/ ³⁹ Ar	³⁶ Ar/ ³⁹ Ar (x 10 ⁻³)	K/Ca	⁴⁰ Ar* (%)	³⁹ Ar (%)	Age (Ma)	±1σ (Ma)
K93-225.5:TRAY C:4 , HBL 1.9 MG, J=0.0145778±0.07%, D=1.0106±0.0027, NM-19, Lab#=2116-01									
X A	800	89.84	0.6103	37.52	0.84	87.7	4.7	1397.2	4.5
X B	950	88.46	3.211	6.150	0.16	98.3	9.8	1496.7	3.5
X C	1020	103.3	8.510	3.908	0.060	99.6	19.7	1679.2	3.5
D	1080	104.9	8.622	3.098	0.059	99.8	64.9	1699.4	3.9
E	1120	104.0	9.375	2.859	0.054	100.0	67.6	1691.6	3.9
F	1150	104.9	10.19	3.829	0.050	99.7	72.1	1698.9	3.8
G	1180	105.0	9.722	3.497	0.052	99.8	76.4	1701.0	3.9
H	1210	105.7	8.070	2.929	0.063	99.8	89.0	1707.3	3.5
I	1240	105.9	9.097	3.572	0.056	99.7	96.6	1708.9	3.6
X J	1280	110.0	11.44	5.573	0.045	99.4	99.5	1749.7	4.1
X K	1350	117.3	11.08	32.02	0.046	92.7	99.9	1743.6	10.6
X L	1650	244.6	11.69	469.0	0.044	43.7	100.0	1725.4	59.4
Integrated age ± 1σ			n=12		0.063			1677.6	3.6
Plateau ± 1σ			steps D-I	n=6			77.0	1701	4
DC-25 H:6:52 #1 , hbl, 1.84 mg, J=0.0154492±0.10%, D=1.0106±0.0027, NM-52, Lab#=6762-02									
X A	800	56.66	3.369	143.3	0.15	25.9	0.6	374.4	17.6
X B	900	75.35	4.162	43.58	0.12	83.5	0.8	1242.6	21.0
X C	1000	96.34	5.798	9.253	0.088	97.7	2.2	1643.7	5.2
D	1030	96.75	5.683	3.039	0.090	99.6	6.5	1669.0	4.0
E	1060	96.74	5.759	2.640	0.089	99.7	17.3	1670.3	3.3
F	1090	97.68	5.773	2.020	0.088	99.9	61.6	1683.0	3.6
G	1120	97.53	5.719	2.175	0.089	99.9	82.9	1680.7	3.8
H	1170	98.12	5.878	4.594	0.087	99.4	87.5	1682.8	4.4
I	1200	97.64	6.097	2.331	0.084	99.8	94.2	1682.2	3.7
J	1250	98.23	6.021	2.598	0.085	99.8	98.9	1687.7	3.9
X K	1300	100.3	6.029	-1.8304	0.085	101.1	99.5	1725.6	12.1
X L	1650	103.1	6.829	22.78	0.075	94.1	100.0	1676.8	13.4
Integrated age ± 1σ			n=12		0.088			1674.1	3.4
Plateau ± 1σ			steps D-J	n=7			96.8	1680	3

ID	Temp/Power (°C)/W	⁴⁰ Ar/ ³⁹ Ar	³⁷ Ar/ ³⁹ Ar	³⁶ Ar/ ³⁹ Ar (x 10 ⁻³)	K/Ca	⁴⁰ Ar* (%)	³⁹ Ar (%)	Age (Ma)	±1σ (Ma)
K94-229-2 N:3:#1:52 , musc, 0.80 mg, J=0.0158134±0.10%, D=1.0106±0.0027, nm-52, Lab#=6817-01									
X A	650	36.21	0.0432	4.497	11.8	96.4	1.2	801.9	2.6
X B	700	66.85	0.0096	1.874	53.0	99.2	2.4	1309.1	3.3
X C	750	77.22	0.0054	0.4840	95.0	99.8	3.2	1455.1	3.8
D	800	84.50	0.0050	1.181	101.8	99.6	6.7	1544.9	3.2
E	825	84.67	0.0052	0.4046	97.7	99.9	9.9	1549.9	3.2
F	850	84.68	0.0064	0.5548	79.5	99.8	13.7	1549.4	3.8
G	875	85.57	0.0016	0.1515	315.4	99.9	19.7	1561.9	3.5
H	900	86.08	0.0026	0.3287	194.2	99.9	30.7	1567.5	5.3
I	925	85.09	0.0026	0.1468	195.4	99.9	40.7	1555.9	3.3
J	950	84.11	0.0031	0.2752	165.9	99.9	46.9	1543.4	3.6
K	975	83.69	0.0042	0.2154	121.4	99.9	51.4	1538.5	3.7
L	1000	83.01	0.0037	0.1345	139.4	100.0	54.6	1530.2	3.6
M	1040	84.15	0.0046	0.1082	112.0	100.0	57.9	1544.5	3.3
N	1080	84.78	0.0057	0.2775	90.0	99.9	62.6	1551.7	3.3
O	1120	85.63	0.0056	0.3776	90.3	99.9	68.7	1561.8	3.3
P	1160	85.76	0.0058	0.5224	88.6	99.8	75.5	1563.1	3.5
Q	1200	85.93	0.0050	0.3531	102.3	99.9	84.6	1565.7	3.4
R	1250	87.20	0.0064	0.1839	79.8	99.9	97.0	1581.7	3.7
S	1300	86.91	0.0492	0.9862	10.4	99.7	98.2	1575.3	4.0
T	1650	85.49	0.1508	1.477	3.4	99.5	100.0	1556.3	3.5
Integrated age ± 1σ			n=20		63.2			1548.0	3.1
Plateau ± 1σ		steps D-T	n=17				96.8	1559	3
K94-229-2 N:5:#1:52 , biotite, 0.89 mg, J=0.0158134±0.10%, D=1.0106±0.0027, nm-52, Lab#=6820-01									
X A	600	22.03	0.0283	3.405	18.0	95.5	3.4	523.8	1.8
X B	650	64.59	0.0501	1.988	10.2	99.1	5.3	1276.6	2.9
X C	700	79.94	0.0131	1.019	39.0	99.6	7.2	1488.2	3.0
X D	750	83.05	0.0068	1.451	75.0	99.5	10.9	1525.9	3.7
X E	800	83.90	0.0031	0.5711	167.0	99.8	16.2	1539.8	3.7
X F	850	85.55	0.0058	0.3751	87.4	99.9	22.9	1560.8	3.6
G	900	85.61	0.0048	0.4531	107.3	99.8	28.4	1561.3	3.3
H	950	85.50	0.0076	0.4116	66.8	99.9	34.0	1560.2	3.8
I	1000	86.21	0.0088	0.3314	57.8	99.9	39.9	1569.2	4.0
J	1050	87.49	0.0061	0.1840	83.0	99.9	50.6	1585.2	3.9
K	1100	87.02	0.0050	0.2587	102.9	99.9	66.1	1579.3	3.8
L	1150	86.11	0.0043	0.2916	119.7	99.9	82.1	1568.1	3.4
M	1200	86.53	0.0091	0.3204	55.9	99.9	92.0	1573.1	3.4
N	1300	86.44	0.0526	0.1383	9.7	100.0	96.3	1572.6	3.8
O	1650	86.81	0.0317	0.8154	16.1	99.7	100.0	1574.7	3.8
Integrated age ± 1σ			n=15		48.1			1534.6	3.1
Plateau ± 1σ		steps G-O	n=9				77.1	1576	3

ID	Temp/Power (°C)/W	⁴⁰ Ar/ ³⁹ Ar	³⁷ Ar/ ³⁹ Ar	³⁶ Ar/ ³⁹ Ar (x 10 ⁻³)	K/Ca	⁴⁰ Ar* (%)	³⁹ Ar (%)	Age (Ma)	±1σ (Ma)
LG-229-3 , Muscovite #1, 0.50 mg, J=0.0153121±0.10%, D=1.0106±0.0027, NM-68, Lab#=8038-01									
X A	750	63.66	0.0912	15.56	5.6	92.8	3.2	1176.3	3.9
X B	800	85.97	0.0230	3.427	22.1	98.8	5.6	1521.4	3.8
X C	840	87.49	0.0185	2.104	27.6	99.3	8.1	1544.6	3.7
X D	880	87.98	0.0107	0.5968	47.8	99.8	10.8	1555.7	4.1
E	920	90.29	0.0077	0.4753	66.2	99.8	26.1	1583.5	3.2
F	960	89.58	0.0074	0.4773	69.2	99.8	38.9	1575.1	3.2
G	1000	87.85	0.0106	0.5918	48.0	99.8	45.7	1554.2	3.3
H	1040	87.40	0.0110	0.2275	46.3	99.9	50.8	1550.1	3.4
I	1080	87.47	0.0130	0.9346	39.4	99.7	55.5	1548.4	3.5
J	1120	87.94	0.0146	1.013	34.9	99.7	61.3	1553.8	3.3
K	1160	88.12	0.0159	0.9862	32.1	99.7	66.3	1556.1	3.5
L	1200	89.40	0.0155	1.355	32.9	99.6	74.9	1570.6	3.4
M	1250	91.59	0.0125	0.3267	40.8	99.9	94.6	1599.2	3.6
N	1300	91.52	0.0857	1.103	6.0	99.7	97.8	1595.9	4.0
O	1650	91.92	0.0878	6.343	5.8	98.0	100.0	1582.4	4.8
Integrated age ± 1σ			n=15		27.7			1561.5	3.1
Plateau ± 1σ			steps E-O	n=11			89.2	1576	3
LG-229-3 , Biotite, pack #3, 0.45 mg, J=0.0152283±0.10%, D=1.0106±0.0027, nm-68, Lab#=8039-01									
X A	650	47.65	0.0471	4.502	10.8	97.2	6.3	974.7	2.7
X B	750	82.75	0.0092	0.8435	55.4	99.7	17.5	1485.8	3.3
C	830	86.88	0.0044	0.4130	115.9	99.9	33.4	1537.5	3.4
D	900	87.34	0.0170	0.3625	30.1	99.9	39.9	1543.2	3.3
E	970	86.20	0.0287	0.8750	17.8	99.7	47.3	1527.7	3.7
F	1050	85.40	0.0154	0.6418	33.1	99.8	56.5	1518.9	3.5
G	1120	84.67	0.0153	0.3922	33.3	99.9	74.5	1510.9	3.7
H	1180	85.42	0.0202	1.047	25.2	99.7	87.7	1518.5	3.4
I	1240	87.72	0.0625	0.6294	8.2	99.8	96.1	1546.9	3.6
J	1350	88.37	0.2068	2.282	2.5	99.3	99.4	1549.3	4.0
K	1650	125.2	0.2957	95.87	1.7	77.4	100.0	1655.1	11.3
Integrated age ± 1σ			n=11		17.8			1493.1	3.1
Plateau ± 1σ			steps C-K	n=9			82.5	1528	3
DC-236-6 #2:B:4:52 , hbl, 1.71 mg, J=0.0157988±0.10%, D=1.0106±0.0027, nm-52, Lab#=6730-01									
X A	700	32.98	0.4822	8.983	1.1	92.1	1.3	715.7	3.6
X B	800	34.38	0.0810	1.556	6.3	98.7	5.5	783.4	2.2
X C	900	40.10	0.1819	1.466	2.8	99.0	9.7	888.5	2.4
X D	1000	67.72	3.023	1.603	0.17	99.7	21.1	1327.0	3.1
X E	1030	76.71	4.130	2.101	0.12	99.6	27.2	1448.6	3.0
X F	1060	85.45	4.161	1.710	0.12	99.8	41.0	1561.0	3.3
X G	1090	86.27	3.838	1.405	0.13	99.9	64.1	1571.7	3.4
X H	1120	71.51	2.520	1.857	0.20	99.5	67.3	1377.3	3.1
X I	1170	70.51	2.756	2.752	0.19	99.5	69.8	1363.8	3.9
X J	1200	77.53	4.587	1.675	0.11	99.8	79.9	1461.7	3.5
X K	1250	78.72	3.060	1.153	0.17	99.9	94.8	1476.4	3.1
X L	1300	76.69	1.626	1.401	0.31	99.6	98.3	1446.5	3.3
X M	1650	82.06	1.916	4.881	0.27	98.4	100.0	1503.0	4.5
Integrated age ± 1σ			n=13		0.16			1430.9	2.9
Plateau ± 1σ			no plateau						

ID	Temp/Power (°C)/W	⁴⁰ Ar/ ³⁹ Ar	³⁷ Ar/ ³⁹ Ar	³⁶ Ar/ ³⁹ Ar (x 10 ⁻³)	K/Ca	⁴⁰ Ar* (%)	³⁹ Ar (%)	Age (Ma)	±1σ (Ma)
LG-237-1 , Biotite, single crystal, 0.36 mg, J=0.0153212±0.10%, D=1.0106±0.0027, nm-68, Lab#=8027-01									
X A	650	74.11	0.0053	11.46	95.6	95.4	1.9	1340.3	4.4
B	750	86.27	0.0006	0.7827	831.0	99.7	17.5	1535.2	4.0
C	830	86.24	0.0015	0.2769	338.9	99.9	36.7	1536.6	3.6
D	900	86.16	0.0048	0.5034	106.1	99.8	50.4	1534.8	3.2
E	970	86.08	0.0071	1.312	71.8	99.6	56.0	1530.9	3.6
F	1050	86.11	0.0077	1.063	66.4	99.6	61.2	1532.3	3.6
G	1120	86.41	0.0034	0.3980	150.9	99.9	79.5	1538.2	3.6
H	1180	85.42	0.0055	0.7865	93.3	99.7	90.3	1524.8	3.4
I	1240	86.24	0.0017	0.4205	294.6	99.9	97.0	1536.2	3.7
J	1300	85.61	0.0071	1.789	71.4	99.4	99.8	1523.6	3.8
K	1650	102.3	-0.0139	55.84	-	83.9	100.0	1531.9	25.0
Integrated age ± 1σ			n=11		148.5			1530.6	3.1
Plateau ± 1σ			steps B-K	n=10			98.1	1534	3
AZ-349 hbl , J4:60, Hornblende, 2.86 mg, J=0.0139204±0.10%, D=1.0106±0.0027, NM-60, Lab#=7383-01									
X A	800	225.3	6.343	238.5	0.080	69.0	0.7	2108.2	31.2
X B	900	77.92	6.322	34.96	0.081	87.4	1.4	1221.5	29.0
X C	1000	91.47	8.242	4.166	0.062	99.4	13.9	1499.2	4.4
X D	1030	102.0	8.950	3.767	0.057	99.6	40.0	1616.8	3.7
X G	1120	95.64	8.596	9.247	0.059	97.9	46.2	1529.5	5.7
X H	1150	102.6	9.087	6.404	0.056	98.9	60.4	1614.4	4.2
J	1300	103.4	8.983	4.086	0.057	99.6	92.3	1630.4	3.7
K	1650	106.0	9.022	19.60	0.057	95.2	100.0	1609.6	5.8
Integrated age ± 1σ			n=8		0.058			1602.1	3.5
Plateau ± 1σ			steps J-K	n=2			39.6	1626	4
AZ-349 , J2:60, biotite, 0.44, J=0.0138873±0.10%, D=1.0106±0.0027, NM-60, Lab#=7382-01									
X A	650	20.81	0.5124	19.85	1.00	72.0	11.5	344.8	2.6
X B	700	92.02	0.2481	28.91	2.1	90.7	14.7	1405.8	4.8
X C	750	94.21	0.1660	10.83	3.1	96.6	19.3	1492.1	4.0
X D	800	104.6	1.958	2.710	0.26	99.4	24.0	1632.5	3.7
X E	850	109.7	0.9332	1.966	0.55	99.5	30.5	1686.0	3.6
X F	900	111.4	0.7683	1.458	0.66	99.7	36.6	1704.3	3.6
X G	970	115.9	0.2902	1.062	1.8	99.8	45.0	1749.2	3.6
X H	1050	119.6	0.3125	0.7929	1.6	99.8	61.5	1784.8	3.5
X I	1120	106.4	0.2358	0.3822	2.2	99.9	82.0	1655.7	3.4
X J	1180	103.1	1.306	1.924	0.39	99.6	89.1	1618.7	3.7
X K	1250	103.4	1.102	1.108	0.46	99.8	97.8	1623.9	3.5
X L	1650	106.5	1.014	10.26	0.50	97.2	100.0	1628.1	5.2
Integrated age ± 1σ			n=12		0.84			1559.1	3.2
Plateau ± 1σ			no plateau						

ID	Temp/Power (°C)/W	⁴⁰ Ar/ ³⁹ Ar	³⁷ Ar/ ³⁹ Ar	³⁶ Ar/ ³⁹ Ar (x 10 ⁻³)	K/Ca	⁴⁰ Ar* (%)	³⁹ Ar (%)	Age (Ma)	±1σ (Ma)
KOO238-2 , E1, NM-128, hornblende, 1.72 mg, J=0.01648±0.09%, D=1.006±0.0014, NM-128, Lab#=51538-01									
X A	3	85.11	4.898	30.94	0.10	89.7	4.0	1490.9	3.7
X B	5	85.57	7.763	4.110	0.066	99.3	41.5	1604.6	2.3
C	6	88.29	8.964	4.677	0.057	99.2	61.3	1638.4	2.8
D	6	88.14	8.720	3.650	0.059	99.6	73.5	1639.9	2.9
E	7	88.43	8.991	4.824	0.057	99.2	76.9	1639.7	3.4
F	7	89.03	8.697	4.480	0.059	99.3	80.2	1647.9	4.0
G	8	87.10	8.559	4.320	0.060	99.3	81.6	1624.4	6.4
H	9	87.86	8.503	4.473	0.060	99.3	86.7	1633.1	2.9
I	9	86.99	8.375	4.244	0.061	99.3	90.1	1623.0	3.6
X J	10	82.01	7.640	5.059	0.067	98.9	92.5	1555.4	4.2
X K	10	60.89	5.361	11.04	0.095	95.3	93.0	1228.9	12.9
X L	13	77.62	7.499	6.834	0.068	98.2	94.5	1490.6	4.9
X M	16	74.51	7.319	7.644	0.070	97.8	95.5	1444.9	6.4
X N	30	90.39	8.655	7.118	0.059	98.4	100.0	1654.8	3.3
Integrated age ± 1σ		n=14			0.063			1612.7	2.1
Plateau ± 1σ		steps C-I		n=7			48.6	1638	2
AZ-89-38 h:4:52 #2 , hbl, 1.40 mg, J=0.0153288±0.10%, D=1.0106±0.0027, NM-52, Lab#=6842-01									
X A	800	38.39	1.578	51.33	0.32	61.1	2.1	560.9	11.5
X B	900	82.37	0.5486	13.67	0.93	95.2	4.9	1441.2	8.0
X C	1000	83.48	1.305	1.510	0.39	99.6	10.1	1501.4	5.0
X D	1030	93.71	6.630	5.170	0.077	99.0	13.5	1619.9	6.8
X E	1060	99.29	19.03	8.520	0.027	99.0	19.3	1693.0	5.6
F	1090	95.12	24.15	7.736	0.021	99.6	32.9	1656.7	4.4
G	1120	95.03	25.80	7.082	0.020	100.0	69.3	1660.7	3.8
X H	1170	93.10	18.99	16.23	0.027	97.6	73.6	1607.7	6.1
X I	1200	92.35	21.16	13.12	0.024	97.7	75.6	1601.7	10.0
J	1250	93.24	24.76	6.665	0.021	100.0	79.7	1640.0	6.3
K	1300	93.79	26.87	7.868	0.019	99.8	86.4	1645.7	5.9
L	1650	96.58	27.35	11.78	0.019	98.7	100.0	1665.6	5.3
Integrated age ± 1σ		n=12			0.023			1624.3	3.6
Plateau ± 1σ		steps F-L		n=5			74.3	1658	4

ID	Temp/Power (°C)/W	⁴⁰ Ar/ ³⁹ Ar	³⁷ Ar/ ³⁹ Ar	³⁶ Ar/ ³⁹ Ar (x 10 ⁻³)	K/Ca	⁴⁰ Ar* (%)	³⁹ Ar (%)	Age (Ma)	±1σ (Ma)
----	----------------------	------------------------------------	------------------------------------	---	------	--------------------------	-------------------------	-------------	-------------

DC-42 musc N2:#1:52, musc, single xstal pristine, 0.45 mg, J=0.0158134±0.10%, D=1.0106±0.0027, nm-52, Lab#=6813-01

X A	650	37.05	0.1042	67.52	4.9	46.2	0.4	437.2	13.8
X B	700	70.82	0.0291	12.63	17.5	94.8	1.0	1320.4	5.6
X C	750	80.42	-0.0589	0.7733	-	99.7	1.6	1495.2	5.8
D	800	82.92	-0.0224	0.8273	-	99.7	3.0	1526.5	4.0
E	825	82.99	-0.0279	0.8902	-	99.7	4.3	1527.1	4.1
F	850	81.96	-0.0156	1.230	-	99.6	6.3	1513.0	3.4
G	875	81.92	-0.0098	0.7319	-	99.7	9.0	1514.3	3.3
H	900	82.25	-0.0028	0.3764	-	99.9	11.4	1519.8	3.7
I	925	83.34	0.0005	0.4790	945.7	99.8	22.5	1533.0	3.4
J	950	82.80	0.0014	0.3976	363.5	99.9	36.0	1526.6	3.3
K	975	82.28	0.0028	4.325	184.8	98.4	42.6	1505.5	3.8
L	1000	80.82	0.0015	0.3972	341.8	99.9	47.0	1501.7	3.1
M	1040	80.70	0.0039	0.7539	130.9	99.7	51.7	1498.9	3.2
N	1080	81.39	0.0030	0.6024	170.1	99.8	56.4	1508.2	3.0
O	1120	81.97	0.0052	-0.1962	98.2	100.1	61.3	1518.4	3.1
P	1160	82.45	0.0043	0.2280	118.3	100.0	69.0	1523.4	3.5
Q	1200	83.17	0.0063	0.0709	80.8	100.0	81.8	1532.4	3.1
R	1250	84.07	0.0075	-0.0684	67.6	100.0	91.6	1544.2	3.4
S	1300	83.84	0.0374	-0.3021	13.7	100.1	94.3	1542.3	3.3
T	1650	85.89	0.4456	0.0169	1.1	100.0	100.0	1567.0	3.6
Integrated age ± 1σ			n=20		17.9			1521.9	3.0
Plateau ± 1σ		steps D-T	n=17				98.4	1526	3

DC-42 O:6:#2:52, biotite, 1.22 mg, J=0.0158505±0.10%, D=1.0106±0.0027, nm-52, Lab#=6823-01

X A	600	26.94	0.0435	7.664	11.7	91.6	4.9	602.5	2.1
X B	650	57.18	0.0293	3.213	17.4	98.4	9.3	1163.5	2.8
X C	700	65.53	0.0091	1.785	56.3	99.2	13.1	1293.0	3.1
D	750	71.48	0.0086	1.152	59.5	99.5	23.1	1378.5	3.7
E	800	73.75	0.0059	0.7871	86.6	99.7	33.0	1410.6	3.4
F	850	74.06	0.0084	0.6944	60.9	99.7	39.7	1415.1	3.3
G	900	71.39	0.0172	0.9396	29.7	99.6	43.9	1378.2	3.2
H	950	69.62	0.0174	1.241	29.3	99.5	48.7	1352.6	3.5
I	1000	70.51	0.0163	1.423	31.3	99.4	55.9	1364.3	3.2
J	1050	72.59	0.0097	0.9925	52.4	99.6	65.8	1394.2	3.3
K	1100	73.37	0.0081	0.8247	62.7	99.7	79.5	1405.3	3.8
L	1150	75.40	0.0078	0.6406	65.6	99.8	88.3	1433.3	3.1
M	1200	75.79	0.0204	0.4541	25.0	99.8	92.8	1439.0	3.4
N	1300	74.05	0.0184	0.4966	27.7	99.8	97.9	1415.8	3.3
O	1650	74.93	0.0444	1.097	11.5	99.6	100.0	1425.2	3.1
Integrated age ± 1σ			n=15		36.3			1354.6	2.9
Plateau ± 1σ		steps D-O	n=12				86.9	1401	3

ID	Temp/Power (°C)/W	⁴⁰ Ar/ ³⁹ Ar	³⁷ Ar/ ³⁹ Ar	³⁶ Ar/ ³⁹ Ar (x 10 ⁻³)	K/Ca	⁴⁰ Ar* (%)	³⁹ Ar (%)	Age (Ma)	±1σ (Ma)
----	----------------------	------------------------------------	------------------------------------	---	------	--------------------------	-------------------------	-------------	-------------

DC-42 Kspar P:4:52, kspar, 1.25 MG, J=0.0157166±0.10%, D=1.0106±0.0027, NM-52, Lab#=6833-01

X A	650	32.83	-0.0040	2.823	-	97.5	2.9	743.4	2.2
X B	650	15.73	-0.0023	0.4446	-	99.2	5.7	399.8	1.2
X C	700	26.33	-0.0025	0.2879	-	99.7	8.5	630.1	1.7
X D	700	46.43	0.0013	0.6185	394.0	99.6	11.5	997.2	2.6
X E	750	64.71	-0.0027	0.1441	-	99.9	13.9	1280.3	2.7
X F	750	70.32	-0.0031	0.3690	-	99.8	16.9	1357.6	3.0
X G	800	73.36	-0.0123	0.0662	-	100.0	19.8	1399.7	3.2
X H	800	72.90	-0.0001	0.3813	-	99.8	23.4	1392.3	3.1
X I	850	72.84	0.0051	0.2206	99.5	99.9	26.7	1392.2	3.3
X J	900	71.67	0.0015	0.3366	350.5	99.9	31.0	1376.0	3.0
X K	950	70.52	-0.0023	0.1557	-	99.9	36.2	1361.1	3.2
X M	1000	70.75	-0.0019	0.2899	-	99.9	42.2	1363.8	3.1
X N	1050	71.15	0.0051	0.4562	100.0	99.8	48.9	1368.5	3.3
X O	1100	70.72	0.0032	0.4296	158.3	99.8	56.7	1362.8	3.1
X P	1150	69.50	0.0057	0.5047	89.3	99.8	66.8	1345.8	3.3
X Q	1200	69.85	0.0036	0.2841	142.6	99.9	80.2	1351.5	3.2
X R	1200	70.31	0.0057	0.3847	89.6	99.8	91.6	1357.4	3.3
X S	1200	71.38	0.0022	0.3870	237.0	99.8	100.0	1371.9	3.1
Integrated age ± 1σ			n=18		290.9			1297.5	2.7
Plateau ± 1σ			no plateau						

KOOGB-4, D10, NM-128, hornblende, 2.18 mg, J=0.01657±0.09%, D=1.006±0.0014, NM-128, Lab#=51536-01

X A	3	74.11	1.039	27.08	0.49	89.3	2.3	1352.5	4.7
X B	5	74.64	8.818	4.039	0.058	99.4	18.4	1469.6	2.7
X C	6	75.83	9.910	3.321	0.051	99.8	31.4	1490.5	2.3
X D	6	74.92	9.401	3.044	0.054	99.8	39.0	1478.4	2.5
X E	7	74.64	10.29	3.128	0.050	99.9	47.2	1475.8	2.7
X F	7	76.39	10.68	3.607	0.048	99.7	55.6	1498.3	2.8
X G	8	75.67	9.692	3.081	0.053	99.8	61.8	1489.0	2.8
X H	9	78.88	10.04	2.850	0.051	100.0	70.0	1533.2	2.3
X J	10	80.15	11.82	3.545	0.043	99.9	75.5	1550.4	2.9
X K	10	75.47	11.34	3.598	0.045	99.8	78.4	1487.0	3.3
X L	13	80.61	10.61	3.719	0.048	99.7	83.9	1553.5	2.9
X M	16	75.73	9.016	2.651	0.057	99.9	88.1	1490.2	2.7
X N	30	81.39	12.34	4.556	0.041	99.6	100.0	1563.5	2.5
Integrated age ± 1σ			n=13		0.051	K2O=0.23%		1501.7	2.0
Plateau ± 1σ			no plateau						

ID	Temp/Power (°C)/W	⁴⁰ Ar/ ³⁹ Ar	³⁷ Ar/ ³⁹ Ar	³⁶ Ar/ ³⁹ Ar (x 10 ⁻³)	K/Ca	⁴⁰ Ar* (%)	³⁹ Ar (%)	Age (Ma)	±1σ (Ma)
KOGB-4 , D8, NM-128, Biotite, 0.76 mg, J=0.01658±0.09%, D=1.006±0.0014, NM-128, Lab#=51535-01									
X A	1	29.65	0.0834	45.28	6.1	54.9	0.5	435.9	4.0
X B	2	43.47	0.0423	18.17	12.1	87.7	1.3	893.7	2.4
X C	2	53.91	0.0229	8.275	22.3	95.5	3.0	1126.4	2.2
X D	3	61.39	0.0149	4.355	34.3	97.9	8.1	1262.2	1.9
X E	3	64.14	0.0117	2.343	43.6	98.9	12.9	1312.3	2.1
X F	4	64.75	0.0128	2.320	39.7	98.9	19.0	1321.4	2.1
X G	4	65.77	0.0153	1.813	33.3	99.2	26.1	1338.5	2.2
X H	5	66.11	0.0195	1.906	26.2	99.2	32.7	1343.1	2.2
X I	5	66.40	0.0427	1.616	11.9	99.3	38.4	1348.5	2.1
X J	6	66.42	0.0306	1.598	16.7	99.3	44.7	1348.9	2.1
X K	6	66.73	0.0274	1.551	18.6	99.3	51.1	1353.5	2.2
X L	7	67.09	0.0705	1.221	7.2	99.5	60.6	1360.2	2.6
M	8	67.40	0.1280	0.9315	4.0	99.6	68.9	1366.0	2.1
N	10	67.66	0.2839	1.010	1.8	99.6	81.0	1369.7	2.0
O	15	67.70	0.0546	0.7159	9.3	99.7	96.0	1371.0	2.7
P	25	68.70	0.7787	1.386	0.66	99.5	100.0	1383.8	2.4
Integrated age ± 1σ			n=16		4.9			1339.6	1.7
Plateau ± 1σ		steps M-P	n=4				39.4	1371	2
KOGB-5 , D7, NM-128, hornblende, 1.97 mg, J=0.01656±0.09%, D=1.006±0.0014, NM-128, Lab#=51534-01									
X A	3	180.7	4.951	73.33	0.10	88.2	0.7	2363.6	6.9
X B	5	96.70	5.088	2.713	0.10	99.6	12.0	1744.9	2.2
C	6	89.08	4.935	1.688	0.10	99.9	41.8	1657.3	2.9
D	7	88.80	4.814	1.668	0.11	99.9	71.6	1653.6	3.1
E	8	88.73	4.861	1.934	0.10	99.8	78.9	1651.9	2.8
F	9	89.53	4.783	1.465	0.11	99.9	83.2	1663.3	2.6
X G	10	88.33	4.681	0.2110	0.11	100.4	84.4	1653.0	3.6
X H	11	91.29	4.839	3.319	0.11	99.3	85.7	1678.1	3.5
X I	12	90.82	5.137	2.449	0.099	99.7	89.0	1676.1	2.7
X J	13	88.81	5.370	3.557	0.095	99.3	89.7	1647.9	4.9
X K	14	89.66	5.960	2.563	0.086	99.7	91.6	1663.0	3.2
X M	20	90.77	5.267	2.521	0.097	99.6	97.4	1675.4	2.6
X N	30	87.68	5.581	4.413	0.091	99.0	100.0	1631.2	3.0
Integrated age ± 1σ			n=13		0.10			1673.3	2.2
Plateau ± 1σ		steps C-F	n=4				71.1	1656	3

Notes:

Isotopic ratios corrected for blank, radioactive decay, and mass discrimination, not corrected for interfering reactions.

Errors quoted for individual analyses include analytical error only, without interfering reaction or J uncertainties.

Integrated age calculated by summing isotopic measurements of all steps.

Integrated age error calculated by quadratically combining errors of isotopic measurements of all steps.

Plateau age calculated by summing isotopic measurements of all steps of plateau segment.

Plateau age error calculated by quadratically combining errors of isotopic measurements of all steps on plateau.

Plateau error is weighted error of Taylor (1982).

X preceding sample ID denotes analyses excluded from plateau age calculations.

Ages calculated relative to FC-2 Fish Canyon Tuff sanidine interlaboratory standard at 28.27 Ma

Decay Constant (LambdaK (total)) = 5.476e-10/a